CHALMERS
UNIVERSITY OF TECHNOLOGY

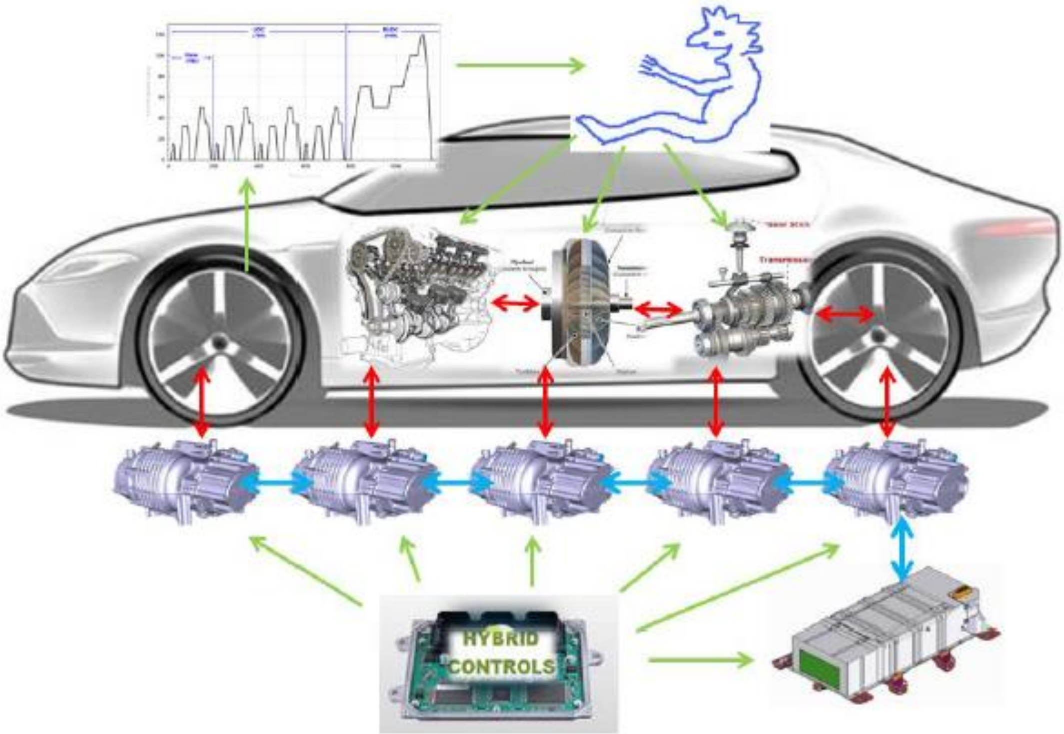

Vehicle Dynamics and Energy Consumption Evaluation Tool

Master's thesis in automotive engineering

Silviu Virgil Margoi
Mahesh Shetkar

Department of Applied Mechanics
CHALMERS UNIVERSITY OF TECHNOLOGY
Gothenburg, Sweden 2017

MASTER'S THESIS IN AUTOMOTIVE ENGINEERING

Vehicle Dynamics and Energy Consumption Evaluation Tool

Silviu Virgil Margoi
Mahesh Shetkar

Department of Applied Mechanics
Division of Vehicle Engineering and Autonomous Systems
Vehicle Dynamics Group
CHALMERS UNIVERSITY OF TECHNOLOGY
Göteborg, Sweden 2017

Vehicle Dynamics and Energy Consumption Evaluation Tool
Silviu Virgil Margoi
Mahesh Shetkar

Examiner: Bengt Jacobson
Supervisors, ÅF: Gunnar Olsson, Meng Yao, Routledge Christoffer
Supervisor, Chalmers: Pär Pettersson

Master's Thesis 2017:11
ISSN 1652-8557
Department of Applied Mechanics
Division of Vehicle Engineering and Autonomous Systems
Vehicle Dynamics Group
Chalmers University of Technology
SE-412 96 Göteborg
Sweden
Telephone: + 46 (0)31-772 1000

Department of Applied Mechanics
Göteborg, Sweden 2017-01-01

Vehicle Dynamics and Energy Consumption Evaluation Tool
Master's thesis in automotive engineering
Silviu Virgil Margoi
Mahesh Shetkar
Department of Applied Mechanics
Division of Vehicle Engineering and Autonomous Systems
Vehicle Dynamics Group
CHALMERS UNIVERSITY OF TECHNOLOGY

Abstract

Regenerative braking systems are a key feature of electric and hybrid vehicles as they allow for significant energy efficiency improvements. However, in certain situations, detailed in the thesis, a mismatch between maximizing the recovered energy and vehicle stability can occur.
The aim of this thesis is to create a high level analysis tool that facilitates the optimization of potential regenerative braking control algorithms, with respect to energy recuperation and vehicle stability. The starting point is a forward dynamics energy model provided by ÅF. Required additions were made in two stages of increasing complexity.
The first part of the project relies on pure longitudinal dynamics simulations. Braking strategies and visualization method are added along with a suitable tire model and idealized traction control and ABS. A modified NEDC cycle is developed with more realistic (aggressive) braking. Evaluation criteria for the vehicle stability are defined. An evaluation method is devised entailing various surface friction simulations for which vehicle stability and energy consumption criteria are computed and visualized.
The second part of the project adds lateral dynamics to the model in the form of a one-track vehicle model. An evaluation method similar with the one in the first part is used, this time with an open loop steering input. The aim is to expand the evaluation of vehicle dynamics and also verify the results from the more simple pure longitudinal simulations.
In both the parts of the thesis a test case comparing two brake distribution strategies is used. The vehicle configuration involves a pure electric, 100 kW, rear wheel drive motor. The main finding is that both the pure longitudinal dynamics model and the more complex model which includes lateral dynamics are successful in capturing the compromises between energy recuperation and vehicle stability for different regenerative braking strategies. Also, the two methods are found to have a good correlation of results. The second model provides additional data such as curvature influence on energy consumption.
Future work recommendations involve testing additional braking strategies and refining the vehicle model to a two track one, with path tracking capabilities.

Keywords: Regenerative braking, vehicle stability, brake force distribution, energy recuperation

Acknowledgements

This thesis was carried out with ÅF and the division of Vehicle Engineering and Automotive Systems at Chalmers. We would like to thank our examiner Bengt Jacobson and supervisor Pär Pettersson from Chalmers for their continuous support throughout the thesis, especially with vehicle modelling and its Simulink implementation.

A special thanks goes to our industrial supervisors: Gunnar Olsson for his technical inputs and constructive feedback and Meng Yao for helping us understand the existing ÅF energy model and implement the thesis deliverables in Simulink.

We also thank Marcus Fasth, the propulsion's team manager, for helping us integrate in to ÅF's work environment. Last but not least we want to thank Ingrid Sjunnesson, Rudolf Brziak and Christopher Routledge from ÅF for their input and suggestions.

Table of Contents

Notations

List of Symbols:

a_x = longitudinal acceleration
a_{xg} = normalized longitudinal acceleration
a_y = lateral acceleration
B = stiffness factor in “Magic Formula”
B_Y = lateral stiffness factor in “Magic Formula”
C = shape factor in “Magic Formula”
C_{Fa} = cornering stiffness
C_{Fx} = longitudinal tire stiffness
C_{Fy} = lateral tire stiffness
$C_{F\kappa}$ = longitudinal slip stiffness
C_Y = lateral shape factor in “Magic Formula”
D = peak factor in “Magic Formula”
D_Y = peak factor in “Magic Formula”
E = curvature factor in “Magic Formula”
E_Y = curvature factor in “Magic Formula”
F_{br} = braking force
F_x = longitudinal force
F_y = lateral force
F_z = vertical force
J = yaw inertia of vehicle
K_{US} = understeer gradient
k_{vlow} = damping factor in the tire model
L_r = tire relaxation length
R = turn radius
r = yaw rate of vehicle
r_{eff} = effective wheel radius
T_{brake} = the brake torque applied on an axle
T_{prop}= propulsion torque on a certain axle
$T_{request}$= torque request from the driver model
u = deformation length
v_{low} = tire damping deactivation speed
V_{sx} = longitudinal slip speed
V_x = longitudinal speed
V_{xw} = wheel translational velocity

List of Symbols (greek):
α = tire slip angle
ψ = vehicle yaw angle
δ = angle at the wheel resulting from steering
μ = road friction coefficient
κ = steady state slip
κ' = transient slip
Ω = wheel rotational speed

σ_{κ} = longitudinal relaxation length

List of subscripts:

F = Front
R = Rear
x = Longitudinal
y = Lateral
z = Vertical
br = brake

1 Introduction

1.1 Background

As a result of the ever increasing targets for CO_2 emissions, the automotive industry is developing and utilizing numerous solutions for improving a vehicle's energy efficiency. One general trend across manufacturers is the increase of the electrification level, resulting in various degrees of hybridization or even fully electrical vehicles. One of the key advantages of this strategy is the possibility to have regenerative braking. This allows for some of the energy, otherwise wasted as heat by the friction brakes, to be recuperated by an electric machine (EM) and being transferred to an energy storage device (battery or supercapacitor).

Ideally, a regenerative braking system (RBS), would utilize all the available inertial energy of the vehicle, without the use of friction brakes. However, limitations on the energy storage system (maximum charging power, capacity, state of charge), EM (torque-speed curve), and safety requirements (system redundancy), require the blending of friction brakes torque along with the RBS. This is supplementing the latter when needed, at the cost of energy losses. The way the braking torque is distributed between RBS and friction brakes and also between individual axles or wheels influences both the recuperated energy and the vehicle's stability and dynamic behavior (Boerboom 2012).

An example of contradicting requirements on the RBS is braking in a corner with a rear electric motor. Maximum recuperation is achieved when braking solely the rear axle (with the motor). However, if the friction limit is reached the vehicle oversteers and stability is compromised. A classical brake system distributes the torque between the axles according to an ideal brake distribution curve (see chapter ….). In this case, significantly less energy can be recuperated due to the front axle having only friction brakes.

In (Boerboom 2012) different control strategies were investigated and was found that up to 90 % of the brake energy from a NEDC cycle could be recuperated (neglecting transmission and EM losses). The paper also looked at stability in low road adhesion ($\mu = 0.5$) while cornering (constant $a_y = 3$ m/s^2) for the same NEDC cycle. The evaluation criteria were the number of ESC or ABS activations occurred during the cycle. Only one ESC activation was recorded, and no ABS activations. The results do not show significant differences in stability in between different control strategies. This may be attributed to insufficiently demanding test cycles.

Apart from RBS, possible efficiency improvements have been found under quasi steady state cornering, with differential lateral torque distribution (DeNovellis et al.). A reduction of vehicle understeering behavior when cornering with a high lateral acceleration (> ~ 0.5 m/s^2) can lead to increase in energy efficiency. This is done by active yaw generation through optimum torque distribution which reduces wheel slip. Longitudinal force distribution is being calculated based on the normal load of the tire, considering nonlinear characteristics of the tire. This strategy was compared with the baseline vehicle with equal lateral torque distribution.

In low friction conditions, the possibility of locking the wheels is substantially increased near the limit of adhesion. In (Mutoh 2012), motor control strategies for vehicles with four independent wheel motors were analyzed. The results showed improvements in vehicle stability in ultra-low friction (mu = 0.1) over ABS slip control. This is due to electric motors ability more accurately control torque and consequently wheel slip. This however requires a good estimation of the friction value and a complex vehicle configuration.

1.2 Problem motivating the project

As mentioned before, the RBS control strategy has an impact on both energy consumption and vehicle dynamics. Optimizing each aspect using separate models within different departments is difficult due to the many common design variables. Also, the time required in this process is adding to development lead times and cost.

1.3 Envisioned solution and objective

In response to the above mentioned challenge, a simulation tool, encompassing both energy consumption and vehicle dynamics aspects is to be created. The objective is to *create a high level analysis tool that facilitates the optimization of potential RBS control algorithms, with respect to energy recuperation and vehicle stability.* The starting point is an existing energy consumption simulation tool developed by ÅF. The desired additions include: modified driving cycles, modeling of lateral dynamics, and an evaluation method of the vehicle's dynamic behavior.
The tool should allow evaluating various drivetrain configurations, such as FWD, RWD or AWD. Furthermore, all the functionalities preexistent in the original simulation tool should be preserved. These include energy consumption analysis for conventional and different types of hybrid/electric powertrains.

1.4 Deliverables

The following items are to be delivered by the end of the thesis project:

- Tool extension to the existing model consisting of longitudinal and lateral vehicle dynamics, for simultaneous simulation of vehicle dynamic performance and energy consumption.
- Modified driving cycles appropriate for combined vehicle dynamic performance and energy consumption testing
- Quantifiable criteria to evaluate the vehicle's dynamic behavior
- Visualization tool to facilitate the assessment of results in relation to relevant key parameters .
- Use case comparing at least two control strategies combined with a limited number of scenarios and vehicle configurations.

1.5 Limitations

- The torque blending between friction brakes and electric motors is done in an ideal fashion (disregarding the response lag that the systems would have)

1.6 Method

The development of the thesis is divided into several stages, with increasing complexity in terms of model and analyzed output. This is to facilitate a gradual understanding of the problem and also allow some flexibility in terms of how much output is obtained within the available time span.

The steps followed in the modeling phase are the following:

- Development of the model to a level suitable for a straight line cycle analysis. The added elements are:
    - modified NEDC cycle with higher decelerations and low adhesion coefficient
    - control block for torque blending and torque distribution (front/rear axle)
    - idealized ABS and ESC systems
    - two control strategies
    - evaluation method for the vehicle's longitudinal dynamic behavior
- Comparison of the control strategies
- Development of the model to a level suitable for cycles with lateral dynamics. The added elements, in addition to the existing ones, are:
    - test procedure with lateral travel (fixed steering turn, same longitudinal speed profile as in the longitudinal only test)
    - evaluation method for the vehicle's lateral dynamic behavior
- Comparison of the control strategies

2 Modelling

As mentioned in the introduction, this thesis aims to develop an evaluation tool, starting from an existing energy consumption model provided by ÅF. In this chapter the capabilities and structure of the existing model are briefly presented. The additions made are then described and motivated.

2.1 ÅF energy model

The model built using MATLAB/Simulink and it is used for performance and fuel economy simulations of vehicles with combustion engine and/or hybrid/electric drive. The simulation approach is “forward looking” (or “driver driven”) meaning that a driver model sends control signals to the engine/brakes in order to follow a certain driving scenario.
Some of the key features of the model are the following:

- flexible configuration, adaptable to different applications
- simple Excel user interface for batch runs
- data structure for parameters and data sets
- suitable for use as plant model in SIL/MIL/HIL (Software In the Loop, Model In the Loop, Hardware In the Loop) simulations, for controls validation.

The use cases can be divided in to energy efficiency simulations and performance and drive quality simulations.

Energy efficiency simulations:

- fuel consumption and CO_2 emissions (fuel)
- energy consumption (electric / fuel)
- driving range (electric / fuel)

Performance and drive quality simulations:

- Launch performance
- Acceleration performance from standing start
- Overtaking performance
- Top speed
- Gradeability
- Part pedal performance

The main components of the model are the following:

- combustion engine
- driver model
- clutch
- transmission
- electric motors
- electric motors controls
- battery
- battery management unit

- hybrid vehicle controller
- wheel (containing brakes, tire model and the wheel force calculation)
- vehicle (containing road resistances and speed and distance integration).

A schematic representation of the structure is represented in Figure 2.1 It can be seen that one or more electric motors can be coupled after the engine, before or after the transmission or independent of the transmission altogether (corresponding, for example, to a FWD car equipped with a rear electric motor).

The scope of this thesis specifies that the vehicle to be analyzed is a pure electric one. This means that the engine, clutch and transmission blocks will not be used or modified.

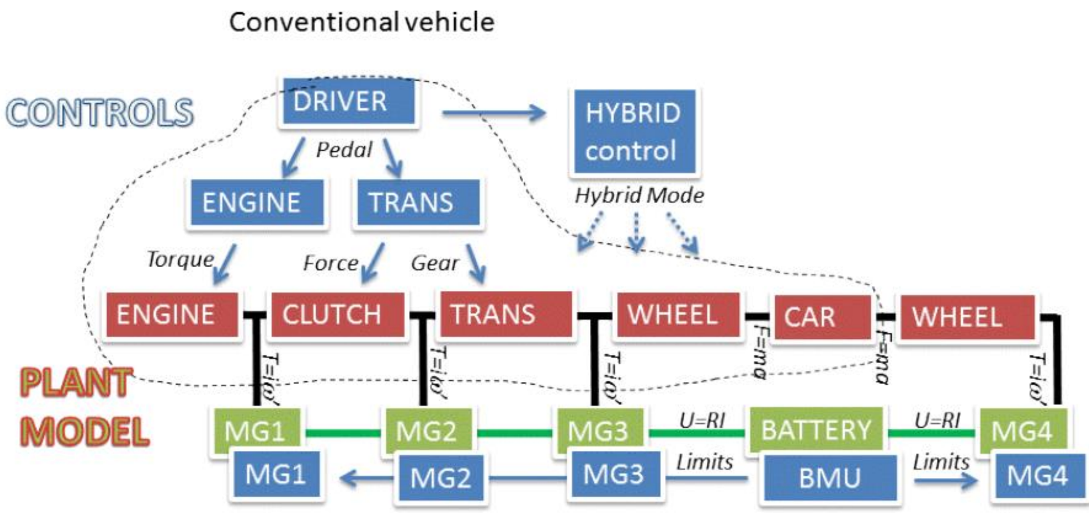

Figure 2.1 Energy plant model structural overview (Sjunnesson, Brziak, and Yao 2015)

Post-processing of the simulation data can be done in Matlab. A large number of signals are saved from Simulink with a sample frequency of 10 Hz. All additional variables added in this thesis work will continue to be saved in the same manner.

2.2 Longitudinal dynamics model

In this section the first part of the modelling (including only longitudinal dynamics) is presented.

2.2.1 Longitudinal load transfer model

Load transfer between the axles/tires may occur under acceleration, braking and cornering situations. Therefore it is important to consider the dynamics of load transfer in analysing the distribution of propulsion/braking forces. The model used in the simulation doesn't include the suspension effects, and is a simple load transfer of a rigid body.

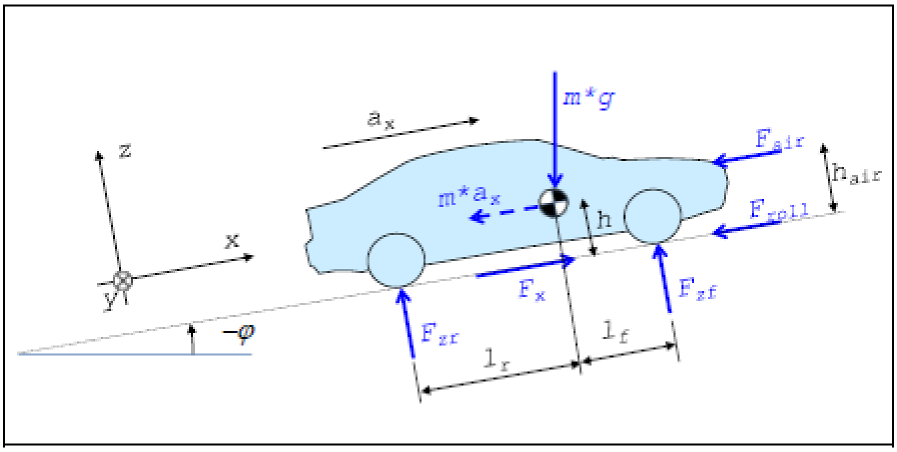

Figure 2.2 Free Body Diagram (Jacobson 2014)

From the moment equilibrium at the rear contact to the ground, load on the front and rear axles are calculated as below.

$$F_{Z_F} = m \cdot \left(g \cdot \frac{l_r \cdot \cos(\phi) + h \cdot \sin(\phi)}{l_f + l_r} - a_x \cdot \frac{h}{l_f + l_r} \right) - F_{air} \cdot \frac{h_{air}}{l_f + l_r} \quad (2.1)$$

$$F_{Z_R} = m \cdot \left(g \cdot \frac{l_r \cdot \cos(\phi) - h \cdot \sin(\phi)}{l_f + l_r} + a_x \cdot \frac{h}{l_f + l_r} \right) + F_{air} \cdot \frac{h_{air}}{l_f + l_r} \quad (2.2)$$

2.2.2 Brake torque distribution

In all automobiles, during braking, the torque is divided between the front and rear axles. The main requirements from this distribution are minimising the braking distance and maintaining the vehicle's stability. Brake regeneration adds maximising energy recuperation as a third requirement and, consequently, creates a link between energy consumption and vehicle dynamics.

2.2.3 Brake force distribution diagram

For a particular vehicle, the interaction between axle braking forces, friction level and deceleration can be represented using only geometric vehicle data and weight distribution. The result is a so called "brake force distribution diagram" and it plays an important role in understanding and designing a brake system (Heißing and Ersoy 2011).

In order to plot the diagram, the vehicle data together with equations (2.3)…(2.10) (adapted from (Boerboom 2012)) are used. Values for the longitudinal acceleration a_{xg} ((g)) and friction coefficient μ ((-)) are given in the form of vectors with values ranging from 0 to 1.2 in steps of 0.1. If needed the ranges could be extended but that is not of interest in the case of regular passenger cars.
If $F_{brR\ ideal}$ and $F_{brF\ ideal}$ from equations (2.7) and (2.8) are plotted against each other a so called "optimal braking curve" or "I curve" is obtained (green curve, see

Figure 2.3). Distributing the braking forces along this curve insures, in theory, that the available friction is fully utilised (minimum braking distance). It also means that a neutral steer behaviour is achieved. A brake distribution “above” this curve results in an oversteering tendency while braking “under” it results in an understeering tendency.

The blue lines from Figure 2.3 represent constant deceleration levels and they are based solely on vehicle mass and total braking force, see equation (2.3).
The almost vertical dotted lines from Figure 2.3 represent the brake distribution at which the front wheels would lock (for a certain available friction). They can be referred to as F lines. To obtain them, U_F and U_R from equation (2.9) are plotted against each other.
The almost horizontal dotted lines from Figure 2.3 represent the brake distribution at which the rear wheels would lock (for a certain available friction). They can be referred to as R lines. To obtain them, O_F and O_R from equation (2.10) are plotted against each other.
The F and R lines delimit the brake operation regions where the following would occur (see Figure 2.3):

- region A: the rear axle wheels are locked
- region B: all wheel are locked
- region C: the front axle wheels are locked
- region D: neither of the wheels are locked

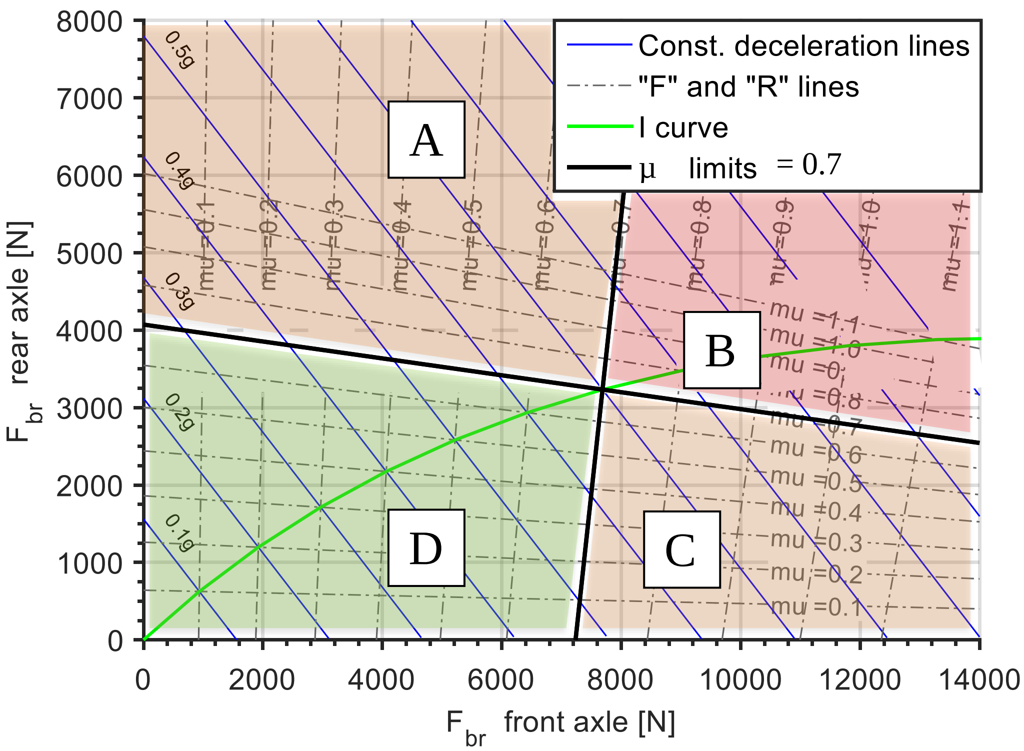

Figure 2.3 Brake force distribution diagram

$$F_{br} = m \cdot a_{xg} \cdot g \tag{2.3}$$

$$P = \frac{F_{brF}}{F_{brR}} = \frac{F_{zF}}{F_{zR}} = \frac{L_R + h_{cog} \cdot a_{xg}}{L_F - h_{cog} \cdot a_{xg}} \tag{2.4}$$

$$F_{brF\ ideal} = P \cdot F_{brR} \tag{2.5}$$

$$F_{brR\ ideal} = \frac{F_{brF}}{P} \tag{2.6}$$

$$F_{brF\ ideal} = \frac{P \cdot F_{br}}{1 + P} \tag{2.7}$$

$$F_{brR\ ideal} = \frac{F_{br}}{1 + P} \tag{2.8}$$

$$U_F = \frac{\mu \cdot h_{cog}}{L - \mu \cdot h_{cog}} \cdot U_R + \frac{m \cdot g \cdot \mu \cdot L_R}{L - \mu \cdot h_{cog}} \tag{2.9}$$

$$O_R = \frac{-\mu \cdot h_{cog}}{L + \mu \cdot h_{cog}} \cdot O_F + \frac{m \cdot g \cdot \mu \cdot L_F}{L + \mu \cdot h_{cog}} \tag{2.10}$$

where:

- m = vehicle mass
- $a_{xg} = \frac{a_x}{g}$ = vehicle deceleration
- g = gravitational acceleration
- P = load proportional brake distribution factor
- F_{brF}, F_{brR} = front/rear axle braking force
- F_{zF}, F_{zR} = front/rear axle loads
- h_{cog} = vehicle centre of gravity height
- L_F, L_R = front/rear distances to the vehicle's centre of gravity
- $F_{brF\ ideal}, F_{brR\ ideal}$ = front/rear braking forces according to the I curve
- μ = road friction coefficient
- U_F, U_R = front/rear braking force for drawing the F lines. Values for U_R can be given between 0 and an arbitrarily chosen maximum
- O_F, O_R = front/rear braking force for drawing the R lines. Values for O_F can be given between 0 and an arbitrarily chosen maximum

2.2.4 Brake force distribution strategies

<u>Linear brake force distribution, ECE regulations</u>

In older vehicles, not equipped with modern electronics, the ideal braking curve cannot be achieved. Instead, the distribution is linear, as a compromise between friction utilisation and vehicle stability (avoiding rear axle lock-up). The linear distribution intersects the "I curve" in a single point. The friction level where the intersection occurs should be situated between μ = 0.15…0.8 (UnitedNations 2011). Such a linear brake distribution is done according to equations (2.11) and (2.12). The β factor insuring an intersection at a certain friction level ($\mu_{intersection}$) is computed

with equation (2.13) In Figure 6.3 such a curve, named "$\beta_{\mu\ intersection}$ curve" is represented for $\mu_{intersection}$ = 0.8. The expected behaviour of a vehicle in this case is that the front wheels lock first for frictions bellow 0.8 and all wheels would lock for friction levels higher than 0.8.
This control strategy has not been simulated in the model but its equations are relevant for the "90% rear bias" strategy.

$$F_{brF} = \beta \cdot F_{br} \tag{2.11}$$
$$F_{brR} = (1-\beta) \cdot F_{br} \tag{2.12}$$

$$\beta_{\mu\ intersection} = \frac{\mu_{intersection} \cdot h_{cog} + L_R}{L} \tag{2.13}$$

<u>Linear brake force distribution, 90% rear bias</u>

In hybrid electric vehicles, solely for the purpose of maximising energy recuperation, the desired control method is to brake only the axle on which an electric motor is mounted (100% rear bias braking in the chosen configuration). The strategy implemented and analysed in this paper is one with 90% rear bias braking, see Figure 2.4. The reason for not using 100% rear bias is to avoid tire saturation for at least high friction surfaces. The stability of the vehicle in this case (especially in low friction) is expected to be significantly worse than for an optimal brake distribution curve.
To generate it equations (2.11) and (2.12) are used with the exception that the distribution factor β is not computed but directly specified at 0.1.

<u>Optimal brake force distribution</u>

Modern vehicles, equipped with EBD (Electronic Brake Distribution) use the ABS system to modulate the brake pressures and follow more or less the optimal braking curve. Such a distribution is also implemented in the model, see Figure 2.4. In theory this strategy would insure the best friction utilisation and vehicle behaviour, at the cost of reduced energy recuperation.
To generate it, equations (2.7) and (2.8) are used, with the exception that the load proportional "P" factor is taken from the instantaneous load transfer occurring in the model.

After distributing the total brake force request in to front and rear axle forces according to one of the two strategies above, the forces are translated in to a front and rear axle torque requests according to equations (2.14) and (2.15)

$$T_{brF\ request} = F_{brF} \cdot r_{eff} \tag{2.14}$$

$$T_{brR\ request} = F_{brR} \cdot r_{eff} \tag{2.15}$$

where:
- $T_{brF\ request}$, $T_{brR\ request}$ = torque requests for the front and rear axle

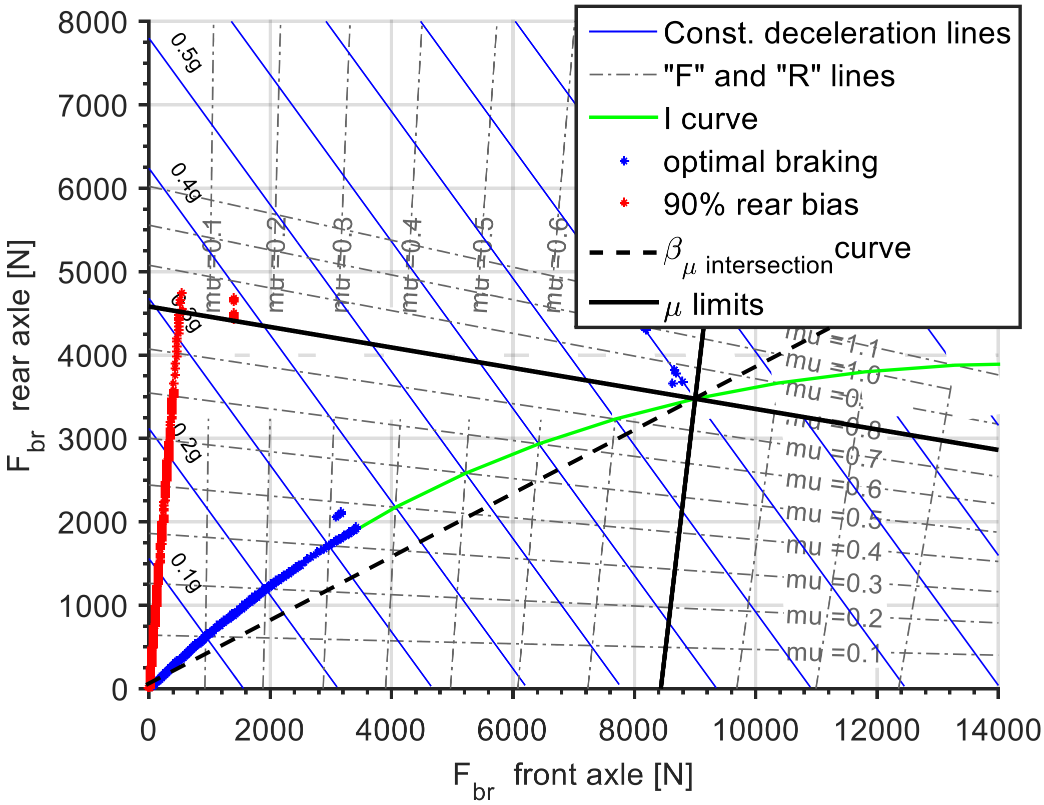

Figure 2.4 Brake distribution strategies. The blue and red curves represent all front/rear braking forces plotted against each other as points, for a modified NEDC simulation (see section 2.2.8)

2.2.5 Brake torque blending

One of the problems with implementing the brake control strategies mentioned earlier is that the electric motor/s (EM) cannot be used to provide all the braking torque in all the required instances. Common limitations are: insufficient maximum torque, decreased efficiency at low speeds or the battery state of charge (SoC-State of Charge) exceeding a certain threshold. Under all these conditions friction brakes have to add to the EM torque or replace it altogether. In practice this is difficult, mainly due to the insufficient response time of hydraulic brakes compared to that of electric motors. However, for the purpose of this paper, it is deemed sufficient to model the brake torque blending in an ideal manner. This is motivated given that the goal is to investigate brake control strategies potential and not the actual implementation of the required mechanical systems.

The logic used for the control is described in the equations (2.16) for the front and (2.17) rear axle. It

$$\begin{gathered} if \quad T_{brF\,request} < T_{EM\,\max F} \\ T_{brake\ F} = T_{brF\,request} = T_{EM\ F} \\ else \quad T_{brake\ F} = T_{EM\,\max F} + \left(T_{brF\,request} - T_{EM\,\max F}\right) \end{gathered} \tag{2.16}$$

$$
\begin{aligned}
&if \quad T_{brR\,request} < T_{EM\,\max R} \\
&T_{brake\,R} = T_{brR\,request} = T_{EM\,R} \\
&else \quad T_{brake\,R} = T_{EM\,\max R} + \left(T_{brR\,request} - T_{EM\,\max R}\right)
\end{aligned} \tag{2.17}
$$

where:

- $T_{EM\,\max F}$, $T_{EM\,\max R}$ = maximum available electric motor torque
- $T_{brake\,F}, T_{brake\,R}$ = brake controller output torque
- $T_{EM\,F}, T_{EM\,R}$ = electric motor torque

The maximum available electric motor torque/s ($T_{EM\,\max F}$, $T_{EM\,\max R}$) is determined taking in to account the energy map, the motor speed and also an ABS activation flag (which sets the maximum EM braking torque to 0, see section 2.2.7).

The above equations are implemented and grouped in the model to form a “brake torque distributor”, see Figure 2.5. The inputs are the electric motor signals and the driver brake while the outputs consist in friction and electric motor brake torques.

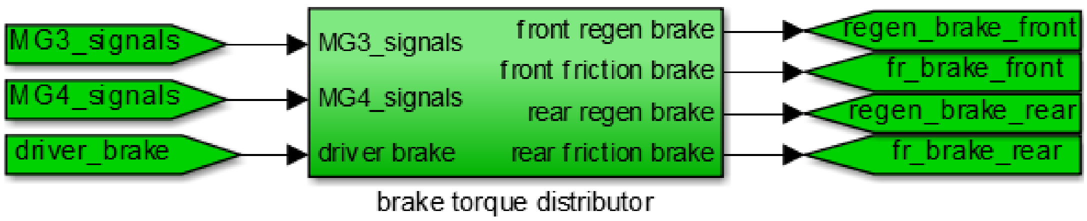

Figure 2.5 High level view of the “brake torque distributor” block in Simulink.

2.2.6 Tire model

<u>Magic formula tire model</u>

Tire characteristics have a crucial influence on the dynamics of a road vehicle (Pacejka 2012). As a result, tire models are an essential element for simulating vehicle dynamics. Depending on the level of detail desired, one or more of the input and output quantities from are used, see Figure 2.6 and Figure 2.7.

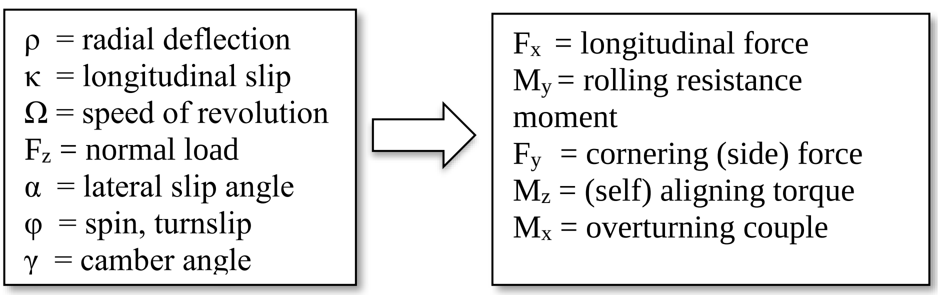

Figure 2.6 Input\output quantities (flat road),adapted from (Pacejka 2012)

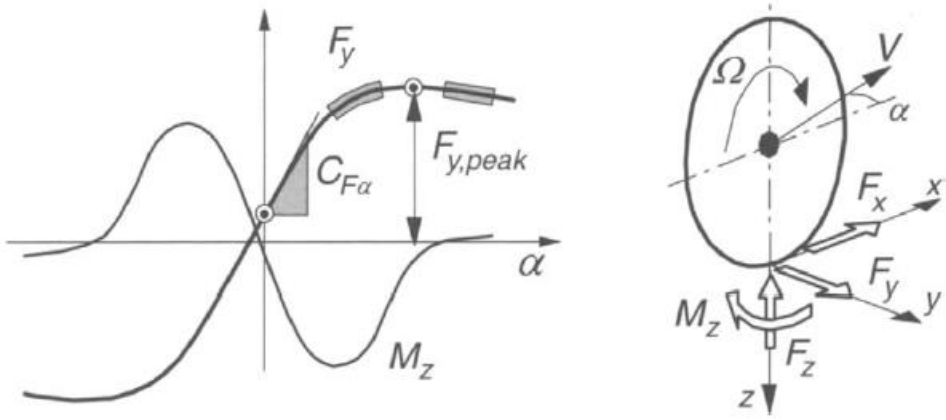

Figure 2.7 Characteristic shape factors (indicated by points and shaded areas) of tire or axle characteristics that may influence vehicle handling and stability properties (Pacejka 2012)

Arguably the most widely used method for estimating the tire forces is the “magic tire” semi-empirical model. The main advantages of this model are:

- tire characteristics easy to fit to experimental data
- tire parameters readily available
- computationally not very demanding
- easy to increase complexity if needed

The main disadvantages are the lack of connection to physical properties and the necessity to have data for each specific tire type and friction level desired.

The tire forces are computed as a function of slip, normal load and tire curve fitting parameters. The number parameters used depends on the level of detail desired. However, in its most basic form, the longitudinal tire force for pure longitudinal slip is given by the set of equations (2.18),(2.19),(2.20),(2.21) and (2.22). A very similar set of formulas can be used to compute lateral forces in the case of pure lateral slip.

Longitudinal force:
$$F_x = D \cdot \{C \cdot \text{atan}\,\{B \cdot \kappa - E \cdot [B \cdot \kappa - \text{atan}(B \cdot \kappa)]\}\} \qquad (2.18)$$

Peak longitudinal force:
$$D = \mu \cdot F_z \qquad (2.19)$$

Stiffness factor:
$$B = \frac{C_{F\alpha}}{C \cdot D} = \frac{C_{F\alpha}}{C \cdot \mu \cdot F_{z\_}} \qquad (2.20)$$

Cornering stiffness:
$$C_{F_\alpha} = B \cdot C \cdot D = c_1 \cdot \sin\left[2 \cdot atan\left(\frac{F_z}{c_{2\_}}\right)\right] \qquad (2.21)$$

Longitudinal slip:
$$\kappa = \frac{V_x - r_{eff} \cdot \Omega}{V_x} = \frac{V_{sx}}{V_x} \qquad (2.22)$$

where:

- μ = friction coefficient
- F_z = normal load
- B = stiffness factor
- C = shape factor

- D = peak factor
- E = curvature factor
- V_x = wheel center longitudinal speed
- r_{eff} = effective wheel radius
- Ω = wheel rotational speed
- V_{sx} = longitudinal slip speed

Single contact point longitudinal transient tire model

One weakness in the method described above lies in the way the slip is calculated. In equation (2.22) one can notice that when V_x is zero the formula is not valid anymore. In simulations a workaround is to set a limit to the denominator, of 1 … 0.1 m/s. However, at low speeds the resulting slip exhibits a highly oscillatory behavior, as seen in Figure 2.11, b). These oscillations were observed to cause both a high simulation time and errors in the energy consumption results. This is of particular interest for this paper due to the fact that energy simulations include sections with zero speed.

The solution adopted is to implement a single contact point, transient tire model, described in (Pacejka 2012) and utilized in papers such as (Boerboom 2012) and (Schmid 2011). The difference from the steady state model is that, instead of steady state slip, a transient slip κ' is used as input for the magic tire formula, see equations (2.23),(2.25) and (2.26). The graphical representation of this model is represented in Figure 2.8

$$\sigma_\kappa \cdot \frac{d\kappa'}{dt} + |V_x| \cdot \kappa' = |V_x| \cdot \kappa = -V_{sx} \tag{2.23}$$

$$\frac{d\kappa'}{dt} = \frac{-V_{sx} - |V_x| \cdot \kappa'}{\sigma_\kappa} \tag{2.24}$$

where:

- σ_κ = longitudinal relaxation length
- κ' = transient slip

$$\sigma_\kappa = \frac{C_{F\kappa}}{C_{Fx}} \tag{2.25}$$

$$\kappa' = \frac{u}{\sigma_k} \tag{2.26}$$

where:

- $C_{F\kappa}$ = longitudinal slip stiffness
- C_{Fx} = longitudinal deformation stiffness
- u = deformation length

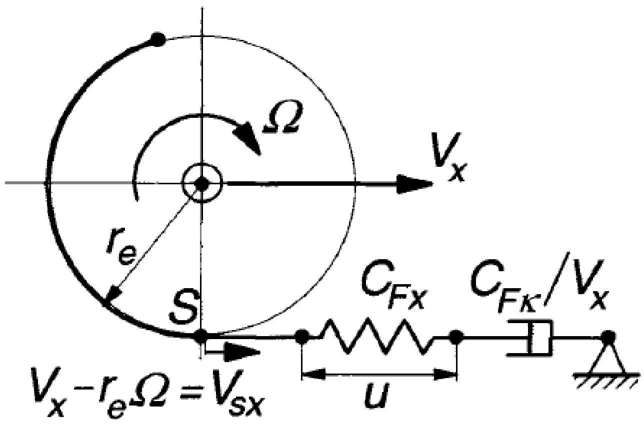

Figure 2.8 Mechanical model of the transient tangential tire behaviour (Pacejka 2012)

Equation (2.24) is implemented in Simulink integrating the state variable κ' (the transient slip).
When used in standstill take-offs, this model gives rise to oscillations which are practically undamped. Normally, damping would be provided by the actual tire material. To mimic this behaviour, equation (2.27) is used to introduce some damping at very low speeds (Pacejka 2012).

$$\kappa' = \left(\frac{u}{\sigma_\kappa} - \frac{k_{vlow}}{C_{F\kappa}} \cdot V_{sx}\right) \tag{2.27}$$

where k_{vlow} is damping factor is given is linearly decreasing from 1000 Nm/s at zero longitudinal speed to 0 Nm/s at $v_{low} = 2$ m/s.

In (Schmid 2011) this type of tire model is simulated for artificially generated slip speed ($V_{sx} = V_x - r_{eff} \cdot \Omega$) and vehicle speed ($V_x$) signals, see Figure 2.9. The scenario assumes a constant acceleration period ($V_{sx} < 0$) followed by coasting ($V_{sx} = 0$) and then braking ($V_{sx} > 0$). The output is the tire slip κ'. In order to verify the tire model from this paper, the same test scenario was recreated, see Figure 2.10,a).

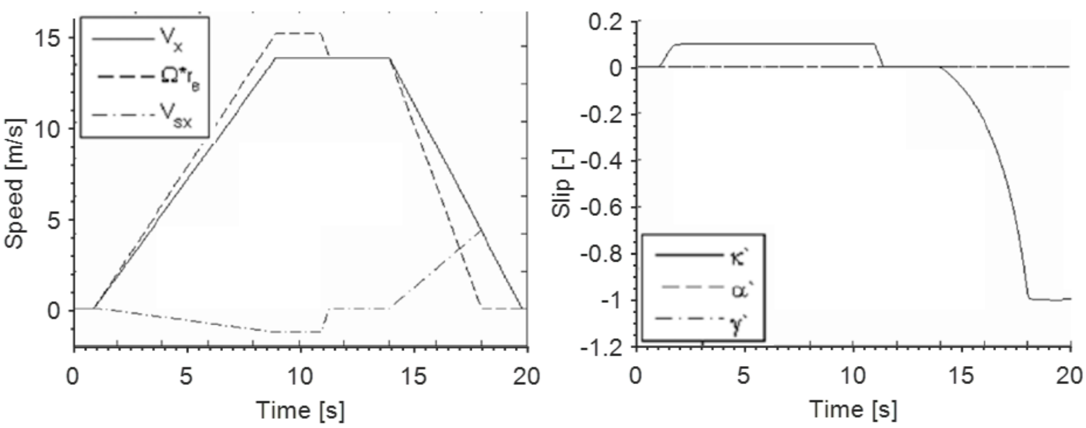

a) *b)*

Figure 2.9 Tire model testing procedure from (Schmid 2011)*: a) Input velocity profiles b) Resulting transient slip κ'*

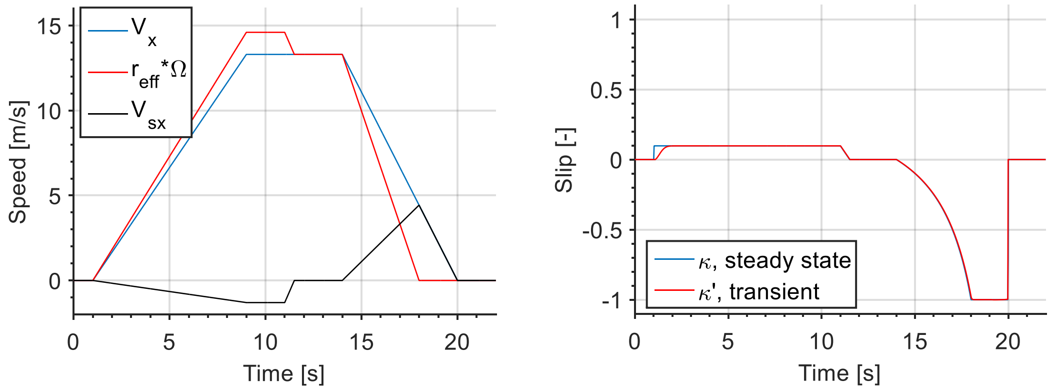

a) *b)*

Figure 2.10 Tire model testing procedure: a) Input velocity profiles b) Resulting transient slip κ'

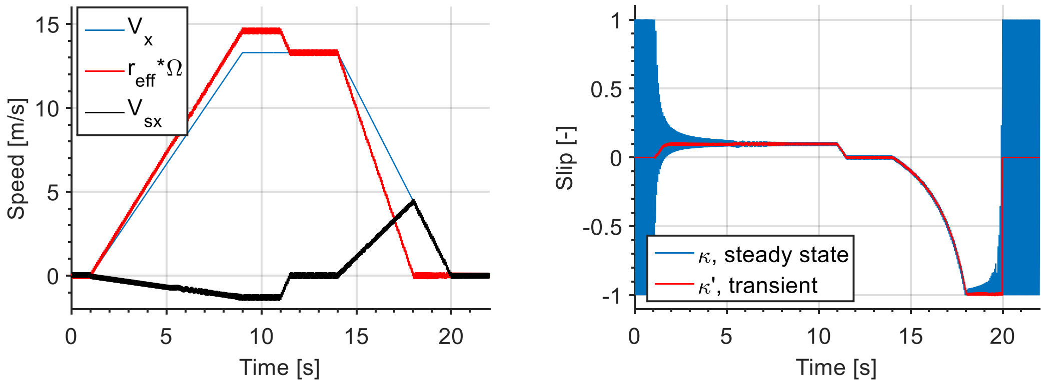

a) *b)*

Figure 2.11 Tire model testing procedure: a) Input velocity profiles with sinusoidal disturbance b) Resulting transient slip κ'

In Figure 2.10 b), the slip for the single contact point transient tire model is plotted, along with that of the steady state model described by equation (2.22). It can be seen that the shape and magnitude of the transient slip is similar to that from Figure 2.9 b), from (Schmid 2011). Also, in Figure 2.10 b), the difference between the transient and steady state slip is made apparent by the lag that the red curve (transient) has, compared to the blue one (steady state), at the start of the scenario. This lag is influenced by the relaxation length σ_κ, defined in equation (2.25). The physical motivation for this behaviour is that it takes some time for the tire to build-up forces when subjected to a torque variation.

As mentioned, a very important benefit of the transient tire model is its stability in low speeds. To demonstrate this, the transient and the steady state models were subjected to similar input signals to those from Figure 2.9 and Figure 2.10, to which a sinusoidal disturbance in the wheel speed, ($r_{eff} \cdot \Omega$), was added (amplitude = 0.2 m/s, f = 15 Hz), see Figure 2.11 a). It can be seen in Figure 2.11 b) that the steady state model (blue line) severally amplifies the disturbance, especially in the low speed areas. The transient tire on the other hand behaves as expected across the entire input speed range, maintaining a similar shape as in the case with no added disturbance in the input signals. This makes the model well suited for carrying out energy consumption simulations.

2.2.7 Traction control and ABS systems

Simulations done in low friction settings revealed that the slip can often reach 100 %, both in driving and braking situations. This impacts the energy consumption values in an unrealistic way considering that modern cars are almost universally equipped with traction control and ABS systems. In response, virtual, idealized versions of these systems are built in to the model, together with the possibility to be switched on or off.

Traction control

A real TCS works by estimating when the wheels are slipping (based on wheel acceleration, front/rear wheel speed difference) and then limiting the propulsion torque so that the slip corresponds to the peak tire force of the tire. Considering that this work is not aimed at designing such a system, the same effect can be obtained by using the equation (2.28). This method works because the load on each axle and the road peak friction coefficient are readily available in the model.

$$T_{prop(i)} = \min\left(T_{request(i)};\ D \cdot F_{z(i)} \cdot r_{eff}\right) \qquad (2.28)$$

where

- $T_{request(i)}$ = the torque request from the driver model for the front or rear axle
- $T_{prop(i)}$ = the propulsion torque for the front or rear axle
- $F_{z(i)}$ = the instantaneous vertical load on the front or rear axle

ABS

The ABS system is implemented in a similar fashion as the TCS, see equation (2.29). In current regenerative braking systems, such as the ones by Bosch, the approach when encountering ABS activations is to fully switch to friction brakes (Bosch). For this reason, the same behaviour was chosen in the present model. This is achieved by having an “ABS activation flag”, which stops the use of the electric motor/motors.The same flag is also used to record how much time the ABS is active, see section 3.1.4.

$$T_{brake(i)} = \min\left|(T_{request(i)}\ ;\ D \cdot F_{z\,(i)} \cdot r_{eff})\right| \qquad (2.29)$$

where $T_{brake(i)}$ = the brake torque applied on the front or rear axle

In Figure 2.12 the difference in slip, between simulations of the full vehicle model with the TC and ABS on, respectively off, is represented. As expected, the TC and ABS limit the slip to around 20% in both accelerating and braking instances. The maximum slip allowed depends on the tire parameters used, more specifically on the slip at which the peak force is produced.

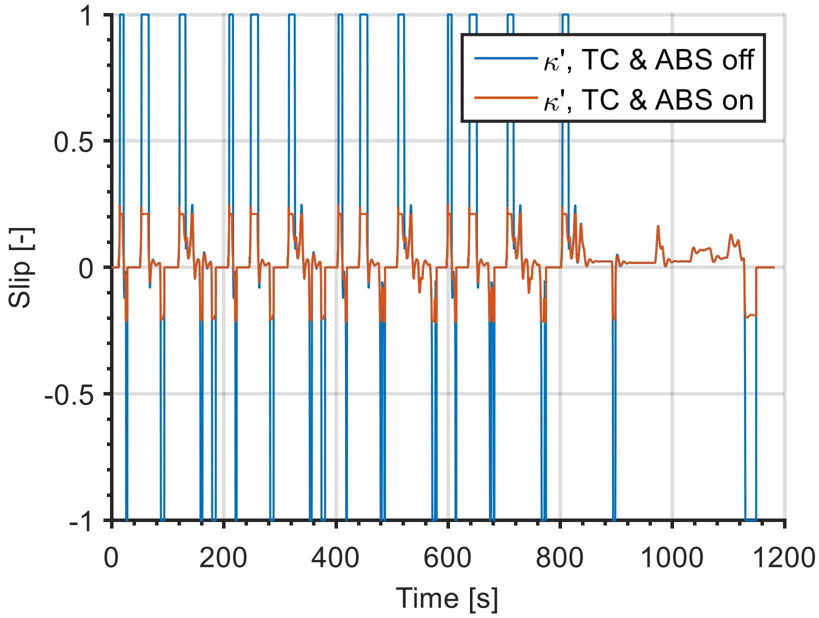

Figure 2.12 Rear wheel slip, RWD configuration, with and without TC and ABS, $\mu = 0.2$.

2.2.8 Driving cycle

At the time of the writing, the most common driving cycle used for energy consumption analysis is the NEDC (New European Driving Cycle). However, a drawback for using it to compare brake regeneration strategies is the relatively mild deceleration values (minimum 1.39 m/s^2). One alternative might seem to be the WLTP (World Harmonized Light Duty Test Procedure), but the minimum deceleration is still only 1.5 m/s^2. Even more, the average deceleration for the NEDC is 0.82 m/s^2 compared to 0.45 m/s^2 for the WLTP (Marotta et al. 2015), which favours the NEDC.
A more suitable driving cycle should cover a relevant percentage of the most common braking scenarios. According to (Heißing and Ersoy 2011), during the lifespan of a vehicle, most braking events occur at decelerations higher than 3 m/s^2, see Figure 2.13. This motivates the assumption that the desired test cycle should have a cumulative brake distribution that resembles the orange portion from the same figure. The solution used to achieve this was to modify the NEDC, which contains four UDC segments (Urban Driving Cycle) and one EUDC segment (Extra Urban Driving Cycle). The modifications were to double the slope (and consequently the deceleration) for the braking portions in the first two of UDC segments and in the EUDC segment. A direct comparison between the modified and the original NEDC is represented in Figure 2.15. One can notice that the accelerating segments remain identical, which means that the total energy used in the cycle remains the same. Differences will appear in the travelled distance and total idling time. However, if desired, an interesting energy consumption comparison with the original NEDC for evaluating the impact of harsher braking, seems feasible.

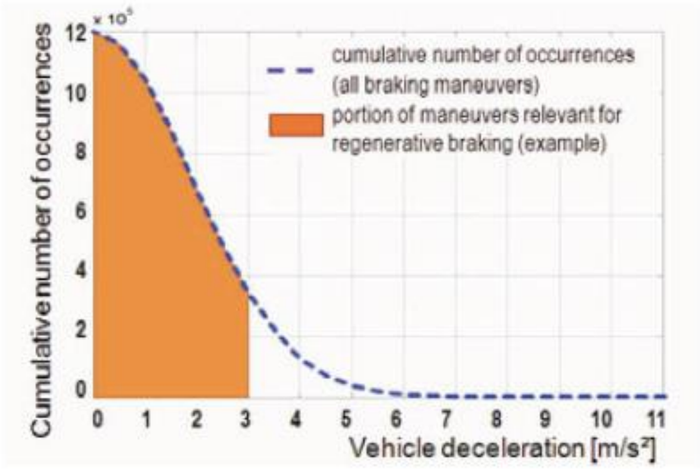

Figure 2.13 Cumulative frequency distribution of braking manoeuvres over a vehicle's lifespan. Regenerative braking potential (up to 3 m/s²) shown for reference. (Heißing and Ersoy 2011)

In Figure 2.14 the distribution of vehicle decelerations for the original and modified NEDC are represented. The "samples" on the y axis are taken from the vehicle acceleration signal, sampled at 10 Hz. It can be seen that the modified NEDC includes the desired range of deceleration (0 … 3 m/s²) and also the shape of the distribution is closer to the desired one, from Figure 2.13. This motivates the use of the modified NEDC cycle for analysing brake regeneration strategies.

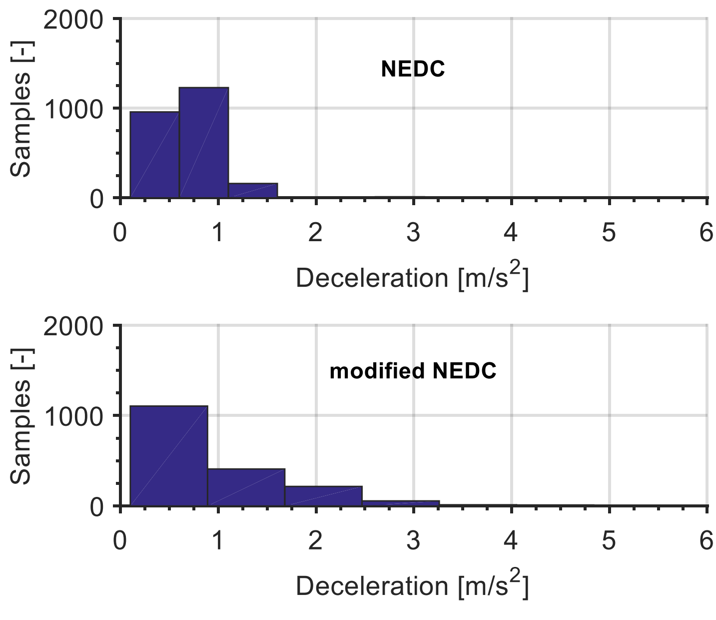

Figure 2.14 Distribution of vehicle deceleration during NEDC and modified NEDC simulations.

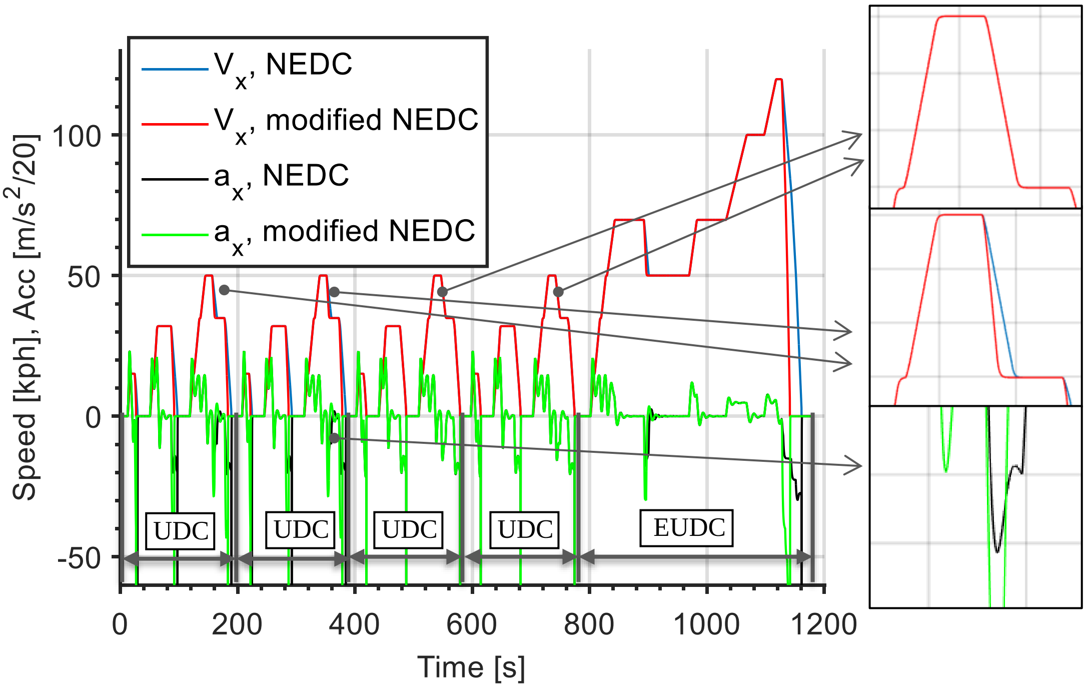

Figure 2.15 Modified vs. original NEDC speed and acceleration.

2.3 Combined longitudinal and lateral dynamics model

The motivation behind introducing lateral dynamics in the existing model is to evaluate stability more efficiently in contrast to the chosen regeneration braking strategy. A comparison of the results will also become possible and it is important to verify that the stability aspects predicted by the previous model are consistent.
The challenge in adding a lateral dynamics model is to secure that the same vehicle is evaluated with both models. Hence the parametrization is to be done carefully, using the same parameter files as far as possible.

2.3.1 One-track vehicle model

A one-track vehicle model is considered and the free body diagram is described in Figure 2.16. The motivation behind using a one-track model instead of a 2 track one is that it allows a much easier extension when starting from the longitudinal dynamics model. This way no additional tires or electric motors have to be added.

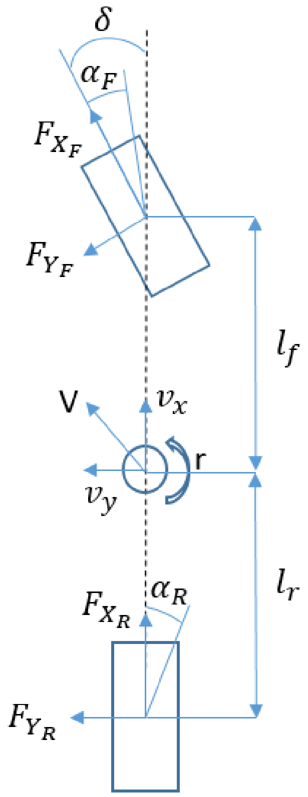

Figure 2.16 Bicycle Model

Rigid planar vehicle motion equations for longitudinal, lateral and yaw dynamics are given in (2.30), (2.31) and (2.32) respectively:

$$F_{X_F} cos\delta - F_{Y_F} sin\delta + F_{X_R} - F_{drag} = m(\dot{v_x} - r \cdot v_y) \qquad (2.30)$$

$$F_{Y_F} cos\delta + F_{X_F} sin\delta + F_{Y_R} = m(\dot{v_y} + r \cdot v_x) \qquad (2.31)$$

$$(F_{Y_F} cos\delta + F_{X_F} sin\delta) \cdot l_f - F_{Y_R} \cdot l_r = J \cdot \dot{r} \qquad (2.32)$$

F_{x_i} and F_{y_i} are the longitudinal and lateral forces for each axle. F_{drag} is the aerodynamic longitudinal drag force. Terms v_x and v_y are the vehicle longitudinal and lateral velocity, m is the vehicle mass, r is the yaw rate, J is the yaw inertia, with l_f and l_r being the distance from front and rear axle to centre of mass respectively. α_F and α_R are the slip angles at front and rear originated from δ at the wheel.

Longitudinal/translational velocity at wheel hub for slip calculation is different from v_x because of the influence of yaw rate and delta.

$$V_{xw_F} = v_x \cdot cos\delta + (v_y + r \cdot l_f) sin\delta \qquad (2.33)$$

$$V_{xw_R} = v_x \qquad (2.34)$$

Lateral forces generated at the tyre are because of the slip angles, and are mentioned below in (2.35) and (2.36)

$$\alpha_F = \delta - \left(\frac{v_y + r \cdot l_f}{v_x}\right) \tag{2.35}$$

$$\alpha_R = -\left(\frac{v_y - r \cdot l_r}{v_x}\right) \tag{2.36}$$

2.3.2 Combined operation tire model

As mentioned in 2.2.6, the tire forces are calculated using Magic Formula Tire Model with longitudinal slip as input parameters. Equation (2.37) is similar to (2.18) in respect to format, but with slip angle as the parameter with changed coefficients to calculate lateral force.

$$F_{Y0} = F_Z \cdot D_Y \sin\left(C_Y tan^{-1}\left(B_Y\alpha - E_Y(B_Y\alpha - tan^{-1} B_Y\alpha)\right)\right) \tag{2.37}$$

As the vehicle model features combined longitudinal and lateral slips, so the forces from pure Magic formula (F_{X0} & F_{Y0}), need to be adjusted using friction circle principle. In equation (2.41) it is specified that the forces may not exceed the absolute peak force capacity of the tire.

$$\sqrt{F_{X0}^2 + F_{Y0}^2} > \mu \cdot F_Z \tag{2.38}$$

Here, μ is the peak friction and F_Z is the load on the tire. If the above condition is true, then the forces (F_X & F_Y) are scaled according to equations (2.39) and (2.40), as given in (Parker, Griffin, and Popov 2016)

$$F_X = F_{X0} \cdot \frac{\mu \cdot F_Z}{\sqrt{F_{X0}^2 + F_{Y0}^2}} \tag{2.39}$$

$$F_Y = F_{Y0} \cdot \frac{\mu \cdot F_Z}{\sqrt{F_{X0}^2 + F_{Y0}^2}} \tag{2.40}$$

2.3.3 Lateral tire relaxation

There is a certain delay in forming the steady state lateral forces after the tire is being introduced by a slip angle, this phenomenon is called tire relaxation. The lateral tire relaxation models same type of dynamics as single contact point longitudinal transient tire model. Together they add the two additional state variables: F_X and F_Y. The following differential equation (2.41) is used to calculate the rate of change in force, which is then integrated back to give out steady state force.

$$\dot{F}_Y = \frac{F_{Y0} - F_Y}{L_r/V_{xw}} \tag{2.41}$$

Relaxation length, L_r is the ratio of Cornering stiffness, C_{Fa} and Lateral tire stiffness, C_{Fy}. V_{xw} is wheel translational velocity. F_{Y0} is the output from the magic formula tire model and F_Y is the lateral tire force after relaxation.

3 Evaluation criteria

In order to reach the objective of this paper it is essential that the vehicle stability is quantified and used to differentiate between different regenerative braking strategies. Criteria for evaluation of vehicle handling/dynamics help to understand the behaviour of a vehicle or to know the limits of handling. It is difficult for a normal driver to predict the limit of tires before actually reaching it, but for engineers it is of importance in order to know the utilizable grip from the tires in a best possible way to make the vehicle safe and predictable for the driver. The following are the different criteria considered for evaluation of vehicle dynamics.

3.1 Longitudinal model

3.1.1 Understeer coefficient

Understeer can be defined as to how much does the driver needs to change the steering input δ to track a radius R with speed V_x increasing (Pacejka 2012), see equations (3.1), (3.2) and (3.3).

$$\left(\frac{\partial\delta}{\partial V_x}\right)_R > 0, \text{ understeer} \tag{3.1}$$

$$\left(\frac{\partial\delta}{\partial V_x}\right)_R < 0, \text{ oversteer} \tag{3.2}$$

$$\left(\frac{\partial\delta}{\partial V_x}\right)_R = 0, \text{ neutral steer} \tag{3.3}$$

The understeer coefficient K_{US} is a function governed by lateral grip available at front and rear, see equation (3.4).

$$K_{US} = \frac{F_{FZ0}}{C_{Fa}} - \frac{F_{RZ0}}{C_{Ra}} \tag{3.4}$$

Here, F_{FZ0} and F_{RZ0} are the static normal load on front and rear axle respectively. C_{Fa} and C_{Ra} are the cornering stiffness's at front and rear based on the available lateral grip (Klomp and Thomson 2011), see equation (3.5). The formula is based under assumption of quasi-steady state longitudinal acceleration, not including the effects of pitch dynamics.

$$C_{Fa} = C_{Fa0}\left(1 - \frac{h \cdot a_X}{l \cdot g}\right)\sqrt{1 - \left(\frac{F_{X_F} \cdot l}{\mu \cdot m \cdot \left(l_f \cdot g - h \cdot a_X\right)}\right)^2} \tag{3.5}$$

Here, C_{Fa0} is the cornering stiffness of the front axle at the static load F_{FZ0} and F_{X_F} is the traction/braking force at front axle. h is the centre of gravity height, l_f is the front axle distance from CoG, l is the wheelbase, a_X is the acceleration, μ is the available peak friction A similar formula is used for the rear axle.

3.1.2 Critical speed

Critical speed is defined when the steady state gain reaches infinity, or in other words, the speed is calculated where either of front or rear axle saturates resulting in understeer coefficient $K_{US} < 0$. Equation (3.6) gives a steady state relation between the steering input δ, curvature $1/R$, understeer coefficient K_{US} and speed V_x.

$$\delta = \frac{l}{R}\left(1 + K_{US}\frac{V_x^2}{g \cdot l}\right) \tag{3.6}$$

Curvature gain is given by equation (3.7), and for the gain to be infinity, the steering input at wheel δ is zero. For this, the critical speed V_{crit} is calculated with equation (3.8).

$$\frac{1/R}{\delta} = \frac{1}{l + K_{US}\frac{V_x^2}{g}} \tag{3.7}$$

$$V_{crit} = \sqrt{\frac{g \cdot l}{-K_{US}}} \tag{3.8}$$

3.1.3 Lateral acceleration margins

The maximum force produced at the tire is influenced by the normal load, which changes continuously because of the load transfer during braking, acceleration and cornering. Due to the combined slip condition, traction or braking forces influence the lateral capacity of the tires resulting in a decreased maximum lateral acceleration of the vehicle.

We can derive the lateral acceleration margins for each axle while considering longitudinal dynamics using equations (3.9) and (3.10) as described in (Klomp and Thomson 2011). Here, $F_{X_{F,R}}$ is the traction/braking force at front or rear axle respectively and $F_{Z_{F,R}}$ is the current normal load on front and rear axle respectively. $\mu_{F,R}$ is the friction resulting from current slip by the magic formula.

$$a_{YF}^{lim} = \frac{l}{m \cdot l_R}\sqrt{\left(\mu_F \cdot F_{Z_F}\right)^2 - F_{X_F}^2} \tag{3.9}$$

$$a_{YR}^{lim} = \frac{l}{m \cdot l_F}\sqrt{\left(\mu_R \cdot F_{Z_R}\right)^2 - F_{X_R}^2} \tag{3.10}$$

The minimum value between the front and rear axle lateral acceleration margins is used as the starting point for an evaluation criteria of the vehicle's stability.

A plot showing the lateral acceleration margin for two different braking strategies, with friction $\mu = 0.3$, is shown in Figure 3.1. The values are computed continuously for the entire cycle. It can be seen that the two curves are identical for the acceleration sections and only differ during braking. The region of interest is the braking which means the acceleration segments can be filtered out. The resulting curves are plotted in Figure 3.2. In order to separate the most critical situations, a further filtering is done which selects only the values for hard braking, with deceleration levels higher than 1 m/s^2. The resulting curves are plotted in Figure 3.3.

For an easy interpretation of the results it is desirable to have a single number attributed to each braking strategy. The solution was to compute a mean lateral acceleration margin for each test scenario. The mean values for the curves from Figure 3.1, Figure 3.2 and Figure 3.3 is mentioned in the legends. It can be observed that the biggest difference between braking strategies is found in Figure 3.3, when filtering out deceleration levels below 1 m/s^2. The latter will therefore be used as an evaluation criteria.

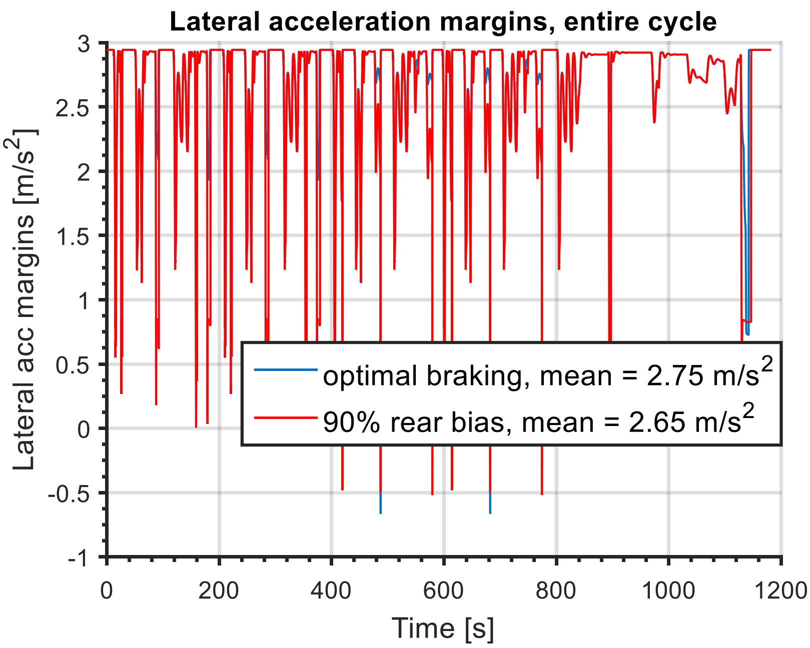

Figure 3.1 Lateral acceleration margins (modified NEDC), entire cycle. Friction coefficient μ = 0.3.

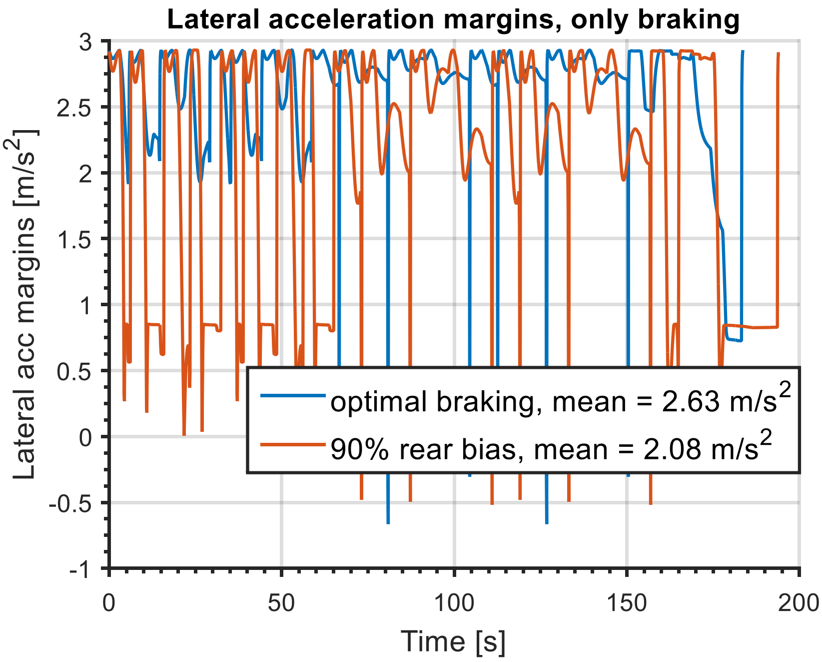

Figure 3.2 Lateral acceleration margins (modified NEDC), only braking. Friction coefficient μ = 0.3.

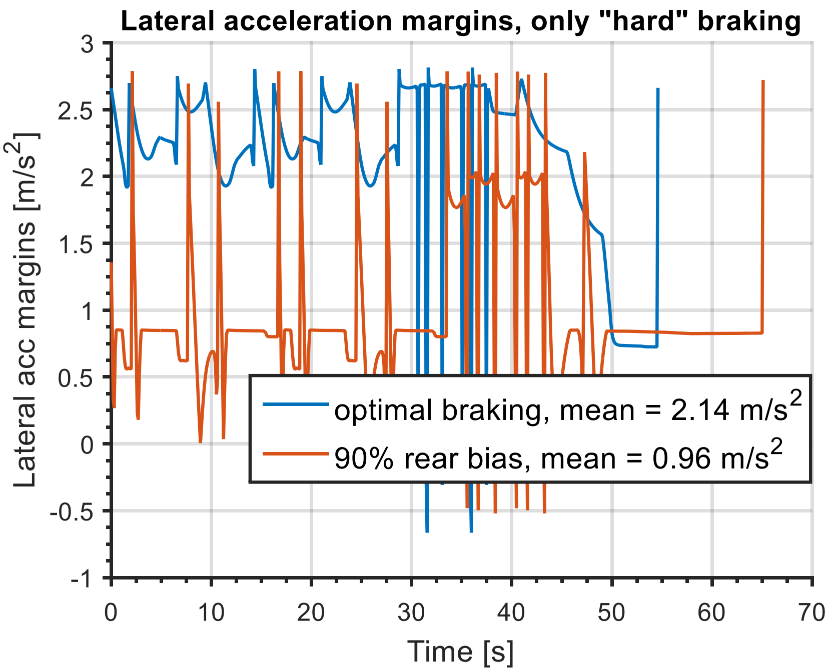

Figure 3.3 Lateral acceleration margins (modified NEDC), only for decelerations higher than 1 m/s^2. Friction coefficient μ = 0.3.

3.1.4 ABS activation time

In section 2.2.7 the modelling of an ABS system from the model was described. In Figure 2.12 the effect of the ABS over slip in low slip conditions was represented. The time for which the ABS is active depends not only on the friction coefficient but also on the type of brake distribution strategy. This leads to the idea that the ABS activation time is a feasible criteria for evaluating the vehicle's behaviour. The interpretation is that a vehicle with more ABS activations would be perceived as less safe/comfortable. It is desirable that the brakes control induces as few unnecessary ABS activations as possible.

Based on preliminary testing and feedback from supervisors, only the “lateral acceleration margins” and “ABS activation time” were chosen as evaluation criteria for the longitudinal model.

3.2 Combined longitudinal and lateral dynamics model

3.2.1 Yaw rate error

When the vehicle model is introduced to a lateral curvature, this evaluation criteria is considered. The curvature chosen for simulations is explained in section 5.2 . A reference yaw rate r_{ref} signal is generated based on the radius R and vehicle speed V_x, given by (3.11)

$$r_{ref} = \frac{V_x}{R} \tag{3.11}$$

The above equation is derived from (3.12) and aiming for a neutral steered vehicle to reduce the number of variables involved.

$$desired\ yaw\ rate, r_{des} = \frac{V_x}{R\left(1 + \frac{K_{US}}{l \cdot g} V_x^2\right)} \tag{3.12}$$

The error is basically the difference between the reference yaw rate r_{ref} and the one achieved from vehicle model r, as given in equation (3.13).

$$r_{error} = r_{ref} - r \tag{3.13}$$

The yaw rate error from (3.13) gives out 3 possibilities, with $r_{error} > 0$ resulting in understeer, $r_{error} < 0$ resulting in oversteer and $r_{error} = 0$ resulting in neutral steer. The mean of the error generated under braking is considered for evaluation.

3.2.2 Saturation Instances

From equations (2.38), (2.39) and (2.40), the total time during braking for which the rear tire forces are scaled down after exceeding the capacity is calculated. This opens up the opportunity to use it as an evaluation criteria for analyzing vehicle stability for different brake strategies.

4 Evaluation method

The main purpose of this paper is to create an evaluation tool that can capture the compromises that arise between energy recuperation and vehicle stability in order to evaluate different brake regeneration strategies.
On one hand, this requires that the model, together with the driving cycle and evaluation criteria is able to capture meaningful data. Assuming this is true, a clear visualisation of the results should also be available for the program's user.

The solution adopted was to create, in the form of several Matlab scripts, a framework from where nine simulations are executed for nine different friction levels (ranging from 1 to 0.2). All nine workspaces generated are saved and all variables are renamed to contain a case suffix and simulation suffix, for example "variable_c1_sim1", variable_c1_sim2,… variable_c1_sim9. This way all data is available if any detailed investigation is required. For a second case the user needs to change the case number, the and the desired vehicle characteristic (in this paper the regenerative braking type but theoretically any other parameter, such as battery or EM size) and re-run the script. The new variables are named "variable_c2_sim1", variable_c2_sim2,… variable_c2_sim9.

The main results are visualized in a combined plot containing both energy consumption data (energy consumption and energy recuperation) together with stability criteria (ABS activation time and lateral acceleration margins). This gives a comprehensive and compact overview of the data.

5 Test Scenarios

5.1 Longitudinal dynamics model

The simulated vehicle is a Saab 93 for which data was readily available. The powertrain considered is a pure electric, 100 kW motor rear wheel drive. Energy maps for the motor together with battery size are also chosen from the available data at ÅF.

5.2 Combined longitudinal and lateral dynamics model

The idea here is to choose the same braking strategies as in previous longitudinal test cases, and add a fixed steering input.
A constant steering wheel input is added during the energy consumption cycle. The following equation (5.1) explains the geometric relationship between wheel steered angle and curvature.

$$\tan(\delta) = \frac{l}{R} \tag{5.1}$$

For having comparable simulations it was important that the acceleration and, even more so, the top speed of the driving cycle are achieved for all the friction conditions (μ = 0.2-1). Therefore, a radius R of 800 m is chosen, which ensures that the vehicle reaches the acceleration and top speed requirements of the cycle while running from low to high friction conditions. By choosing a constant radius R, the vehicle is trying to traverse a circular path but following the energy cycle acceleration requirements.

6 Results

6.1 Longitudinal dynamics model

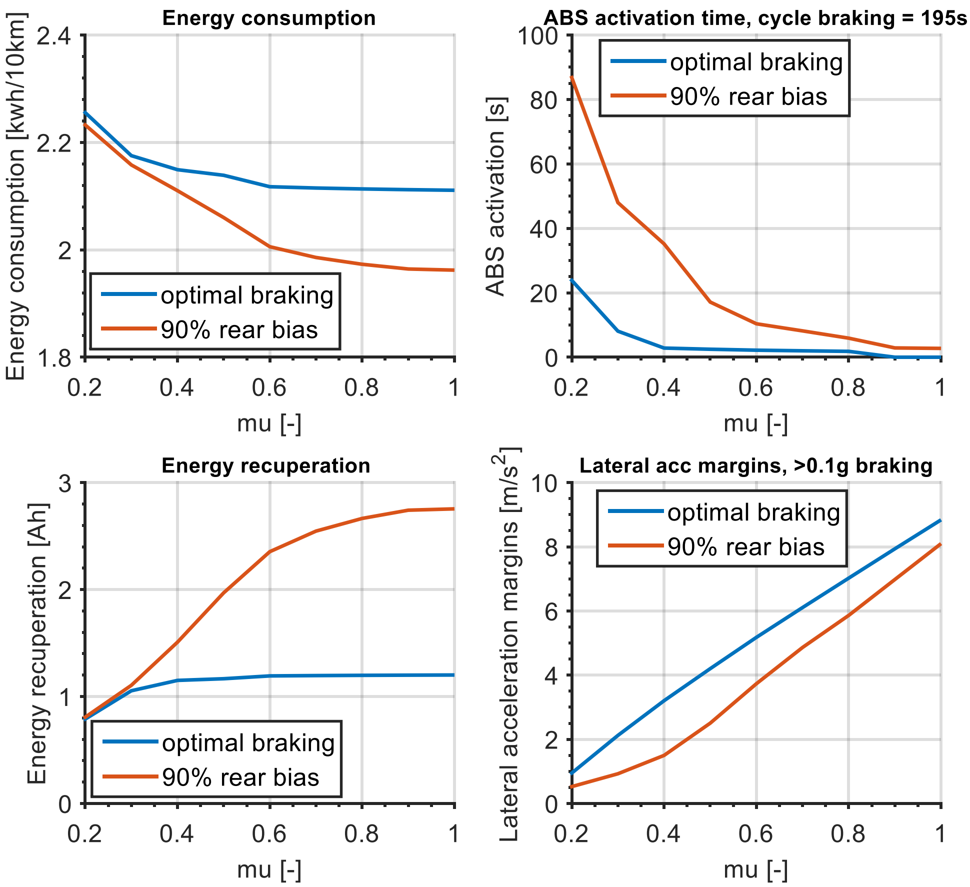

Figure 6.1 Results, modified NEDC

In the figure above an overview of the results is presented. The layout of the 4 subplots is intended to describe energy utilisation on the left side and vehicle stability on the right side.

Energy recuperation in high friction is more than double for rear bias braking than for optimal braking. The numbers go down once the friction decreases, first for the rear bias braking (at $\mu \sim 0.8$) and then for optimal braking as well (at $\mu \sim 0.4$) and they eventually the two tested strategies have a similar performance for very low friction ($\mu = 0.3 \ldots 0.2$).

Energy consumption is lower for rear bias braking in high friction. As friction decreases both strategies show an increase in consumption and also the difference between them becomes small. This behaviour is correlated with the energy recuperation values.

ABS activation time increases for both strategies as friction decreases. The values for rear bias braking are however higher across the friction range. For $\mu = 0.2$ the activation time for rear bias braking is around 90 s while for optimal braking it is only around 20 s. The total braking time in the cycle is 195 s.

The lateral acceleration margins are overall lower for the rear bias braking. In absolute terms the difference between the two strategies is relatively constant across the friction range. A significant relative difference however is observable, see Figure 6.2

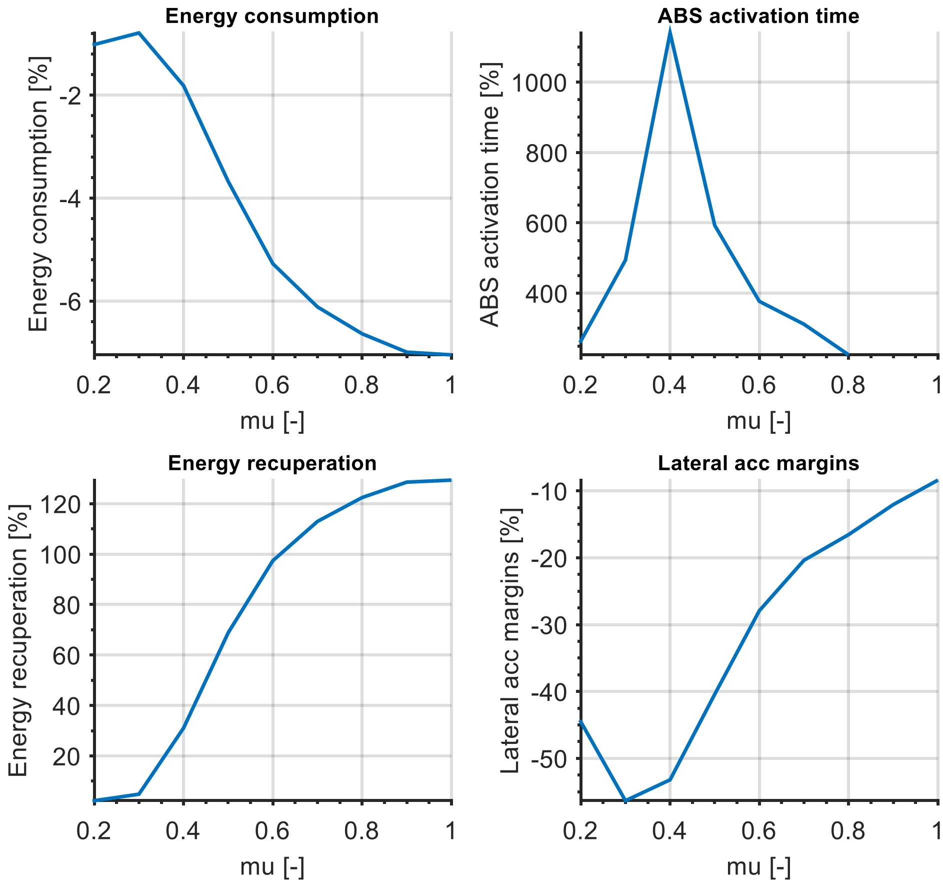

Figure 6.2 Relative difference between the two brake distribution strategies. The line is given by: $\frac{\text{“90\% rear bias”} - \text{“optimal braking”}}{\text{“optimal braking”}} \cdot 100$

In Figure 6.2 the relative difference between the “90% rear bias” and the “optimal braking” strategies is represented in percentages according to equation (6.1).

$$Relative\ difference = \frac{\text{“90\% rear bias”} - \text{“optimal braking”}}{\text{“optimal braking”}} \cdot 100 \qquad (6.1)$$

Energy recuperation is more than 120% higher in high friction for the rear bias braking. However, in low friction the difference goes down to almost 0%.
Energy consumption is more than 6% lower in high friction for the rear bias braking. In low friction the difference goes down to almost 0%.
The relative difference in ABS activation time is not properly defined by the formula used to calculate the ratio. For this reason, in high friction, when the optimal braking strategy has an ABS activation time of zero seconds no values are displayed. In lower friction ($\mu < 0.9$) values can be computed but the values are very high (up to 1000% relative difference).
A significant decrease in lateral acceleration margins is noticeable as friction decreases. This occurs despite the absolute difference (see Figure 6.1) staying relatively constant. The explanation is that the overall lateral acceleration margin is

decreasing along with the friction. Assuming no braking or accelerating, the lateral acceleration margins from equations (3.9) and (3.10) is equal to $\mu \cdot g$ (friction coefficient multiplied by the gravitational acceleration).

6.2 Combined longitudinal and lateral dynamics model

In Figure 6.3, the overall results of energy analysis and evaluation criteria are plotted for two different brake strategies. Each of the plots are explained in the further following sections

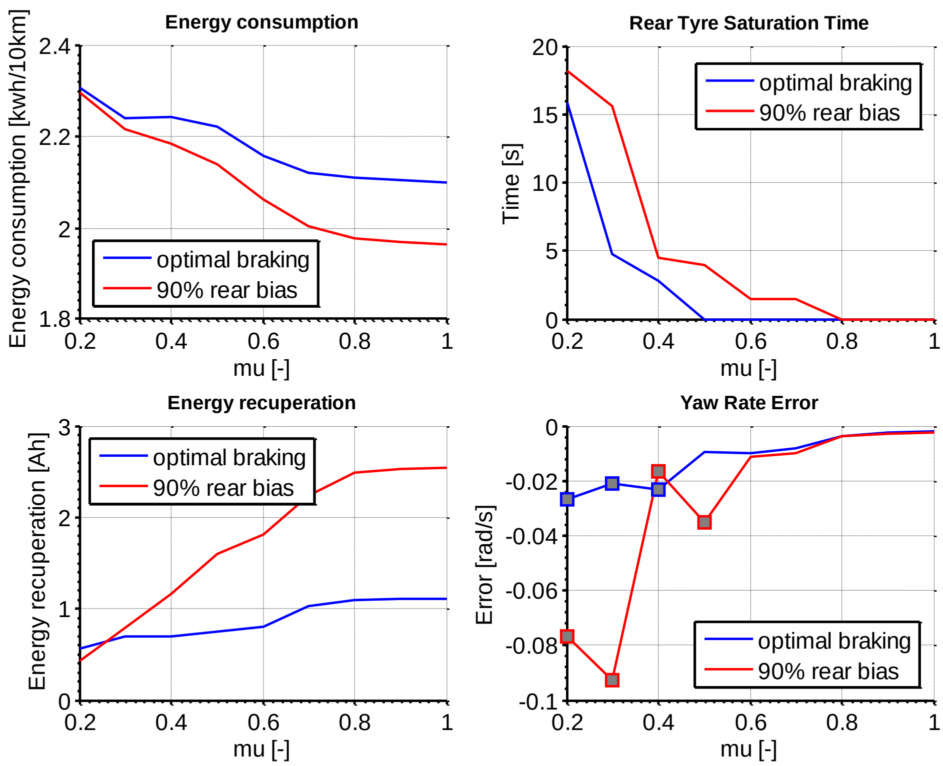

Figure 6.3 Results(Longitudinal + Lateral)

In Figure 6.4 modified NEDC speed profile is being plotted. For comprehensive understanding of results, the cycle is being divided into two sections. Initial 2/3rd part of the cycle, named as low speed section, where vehicle reaches a maximum speed of 50 kph. In the final part of the cycle, named as high speed section, the vehicle reaches a maximum speed of 120 kph, with the average speed being higher than the maximum speed of the low speed section of the cycle.

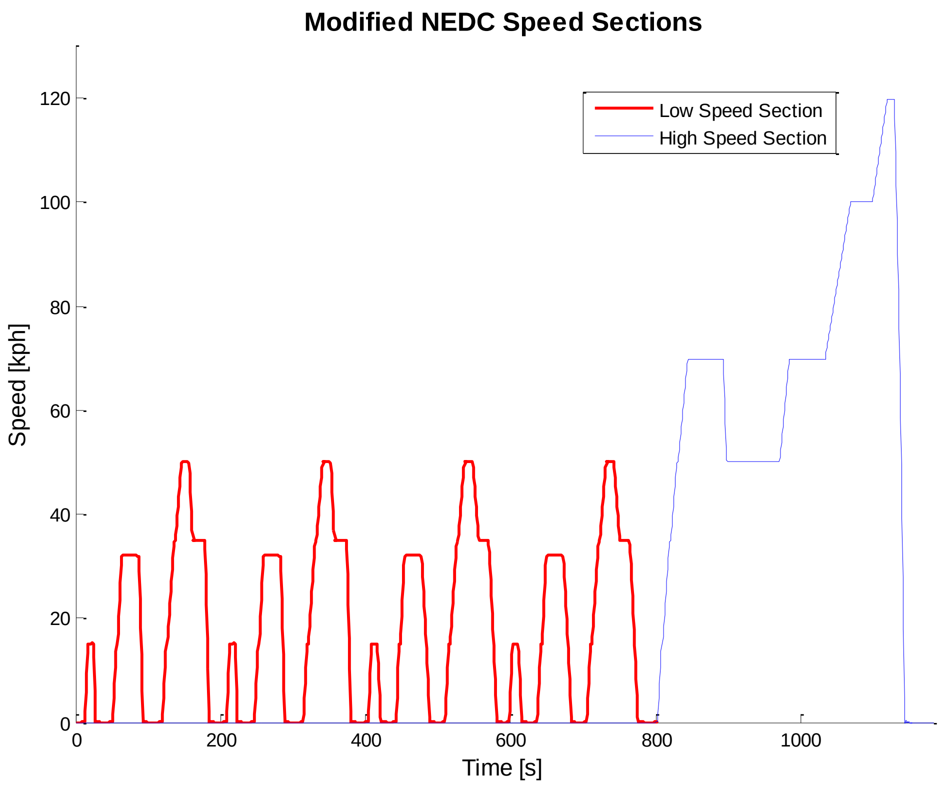

Figure 6.4 Modified NEDC speed sections

In Figure 6.5, yaw rate error curves for simulation with optimal braking strategy are plotted. Only the braking samples in low speed section of modified NEDC are considered with μ ranging 0.2-0.5. It can be seen that as the friction drops error increases making the vehicle comparatively more oversteered. The same trend can be observed in Figure 6.6 as well with μ ranging 0.6-1 for the same braking strategy.

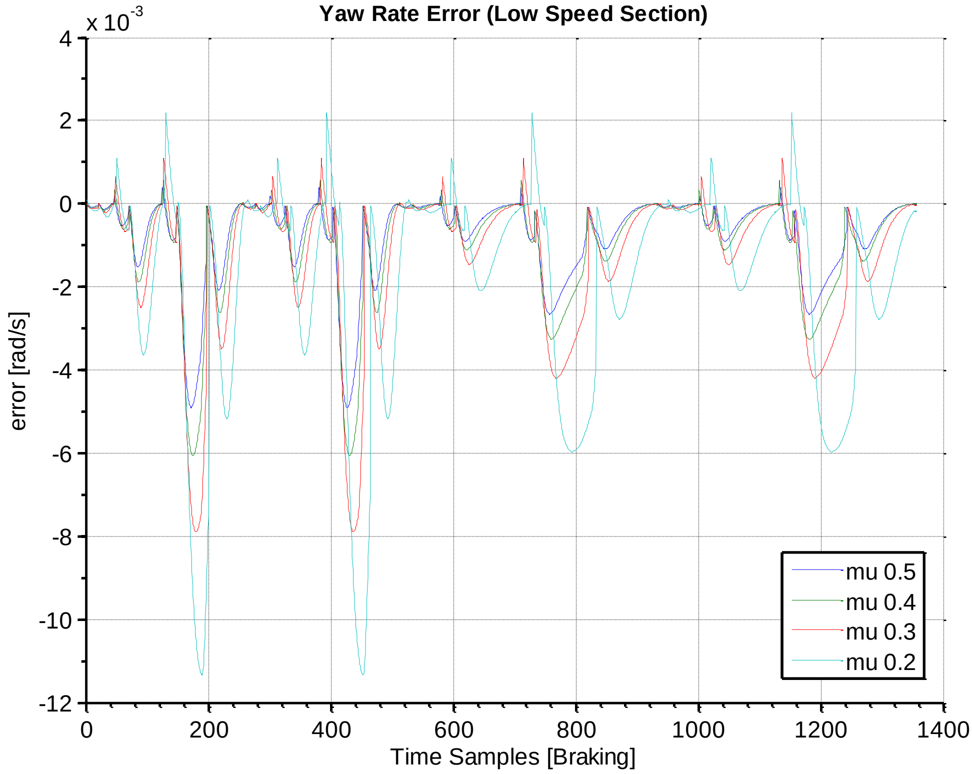

Figure 6.5 Yaw Rate Error with optimal braking strategy (mu 0.2-0.5)

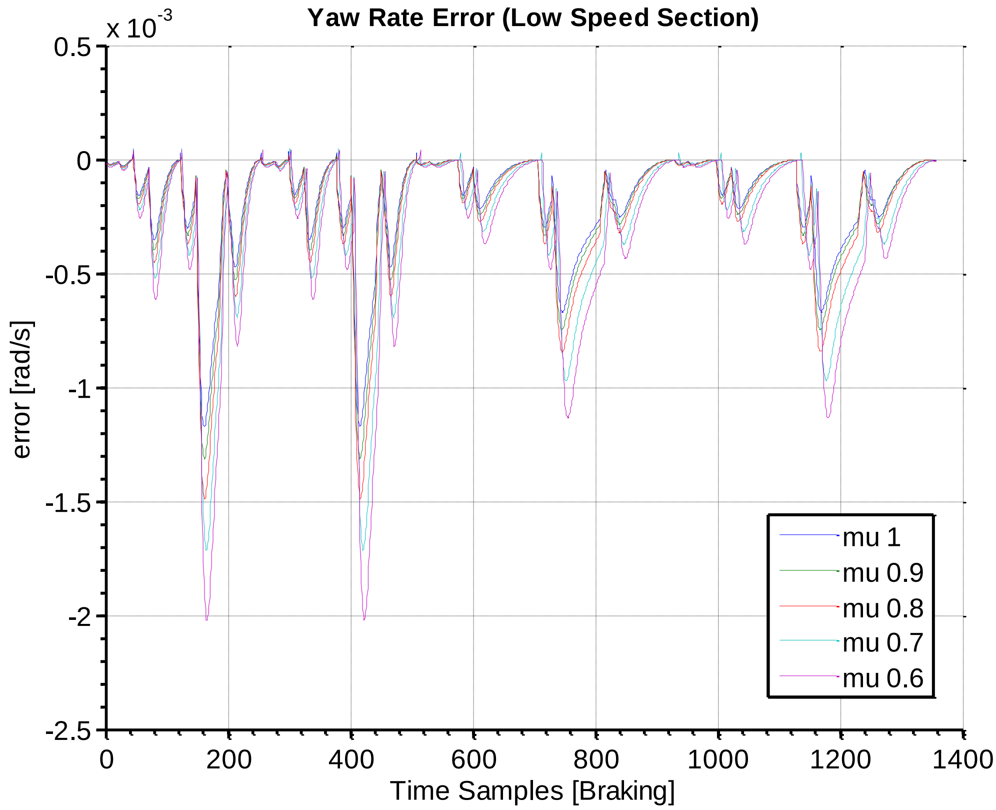

Figure 6.6 Yaw Rate Error with optimal braking strategy (mu 0.6-1)

In order to simplify the results from above plots, mean of the yaw rate error curve from each friction condition is calculated and compared with the other braking strategy of 90% rear biased and is being plotted in Figure 6.7. The following plot gives a clear understanding of the influence of each braking strategy for a corresponding friction condition in the low speed section of the modified NEDC.

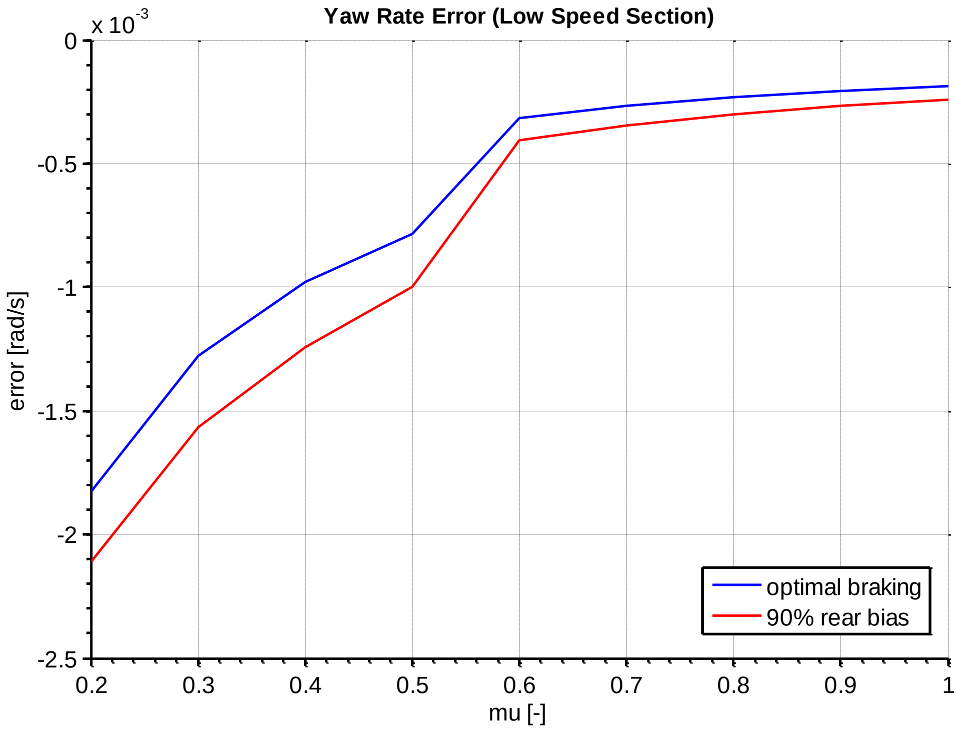

Figure 6.7 Yaw rate error mean for different friction conditions (Low Speed)

The following Figure 6.8 is plotted same as Figure 6.7 but for the high speed section of modified NEDC. Marked results for friction μ ranging 0.2-0.5 for 90% brake bias and 0.2-0.4 for optimal braking indicate that vehicle spins under braking from maximum speed, and as a result mean of the yaw rate error fluctuates and produces unreliable results.

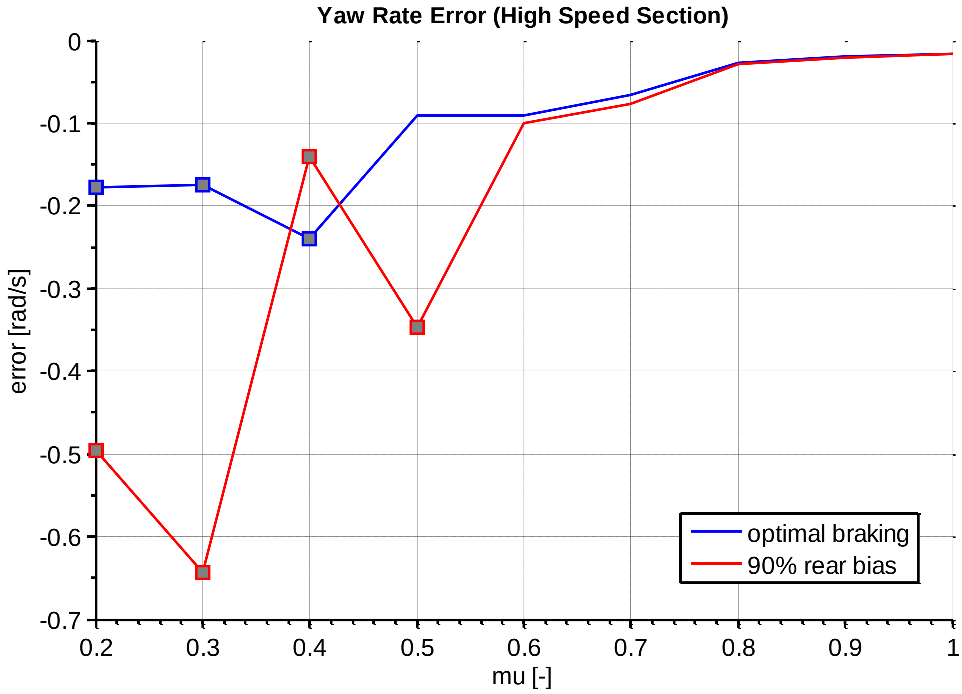

Figure 6.8 Yaw rate error mean for different friction conditions (High Speed)

To get a better understanding and visualization of the marked results as shown by Figure 6.8, the path trajectory and vehicle orientation plot of Figure 6.9 is used. Figure 6.9 corresponds to simulation set up with μ 0.4 and 90% rear bias braking strategy. Start and end of the simulation are also indicated.

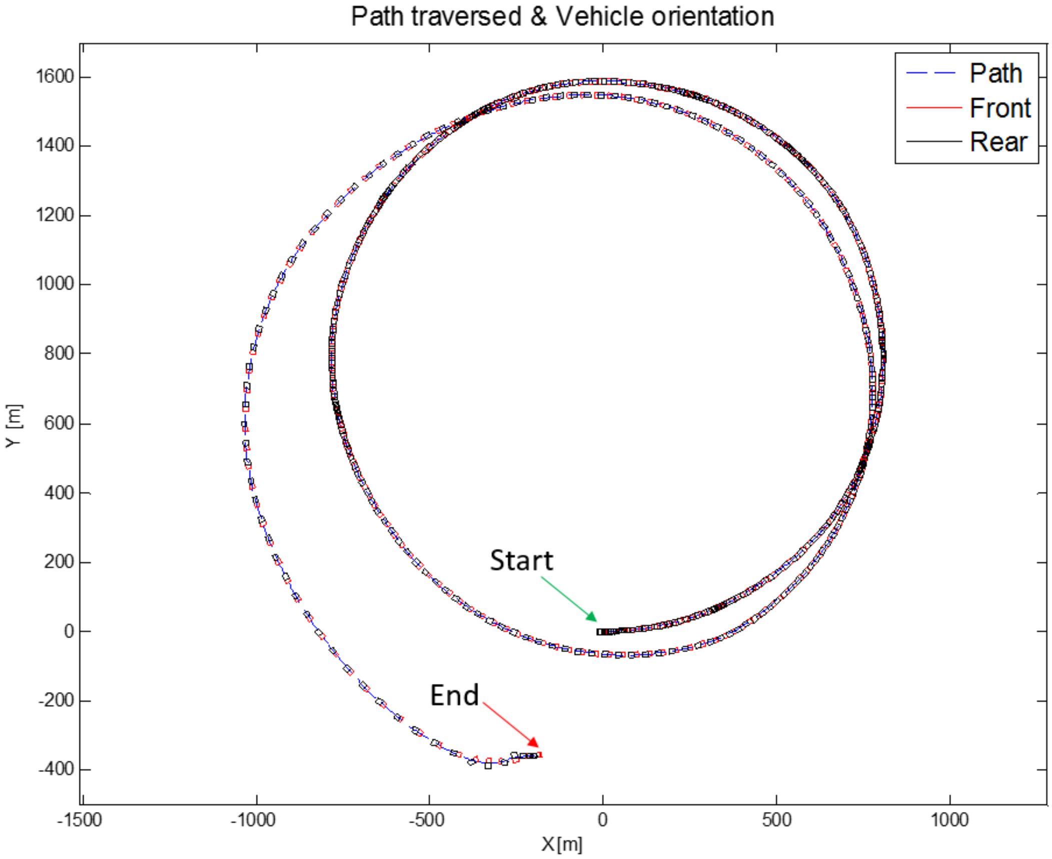

Figure 6.9 Travelled path by vehicle in μ 0.4 with 90% rear bias braking strategy

Taking a closer look during the end of the simulation from above Figure 6.9, it can be seen from below Figure 6.10 that the both of the axles saturate and result in spin under the influence of a fixed steering input.

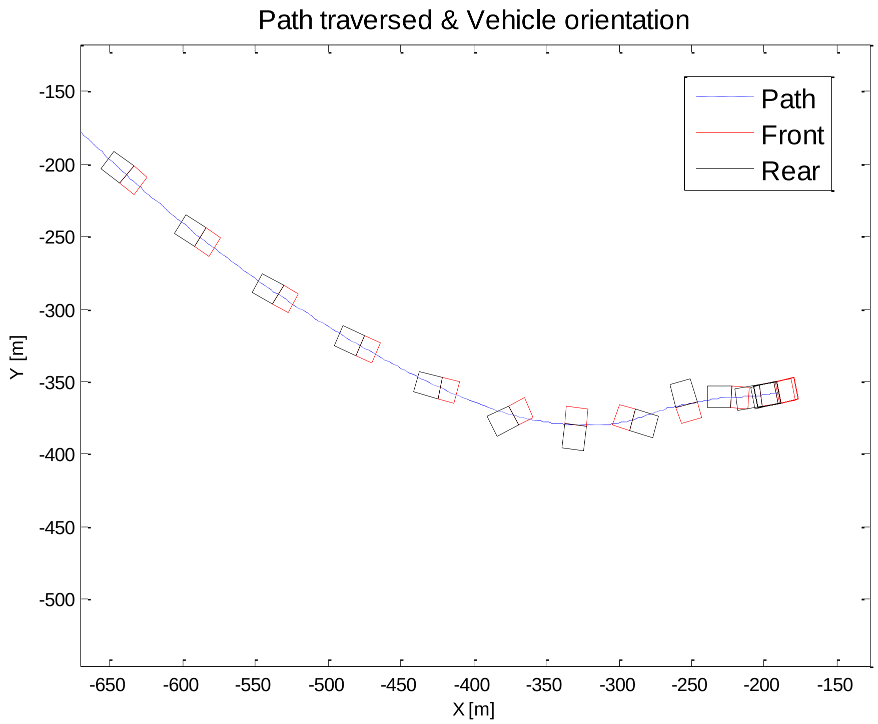

Figure 6.10 Vehicle spinning in μ 0.4 with 90% rear bias braking strategy

The following Figure 6.11 shows velocity components of the vehicle illustrating instability caused under braking from maximum speed as depicted in Figure 6.10. The notations of speed and velocity are as described by Figure 2.16.

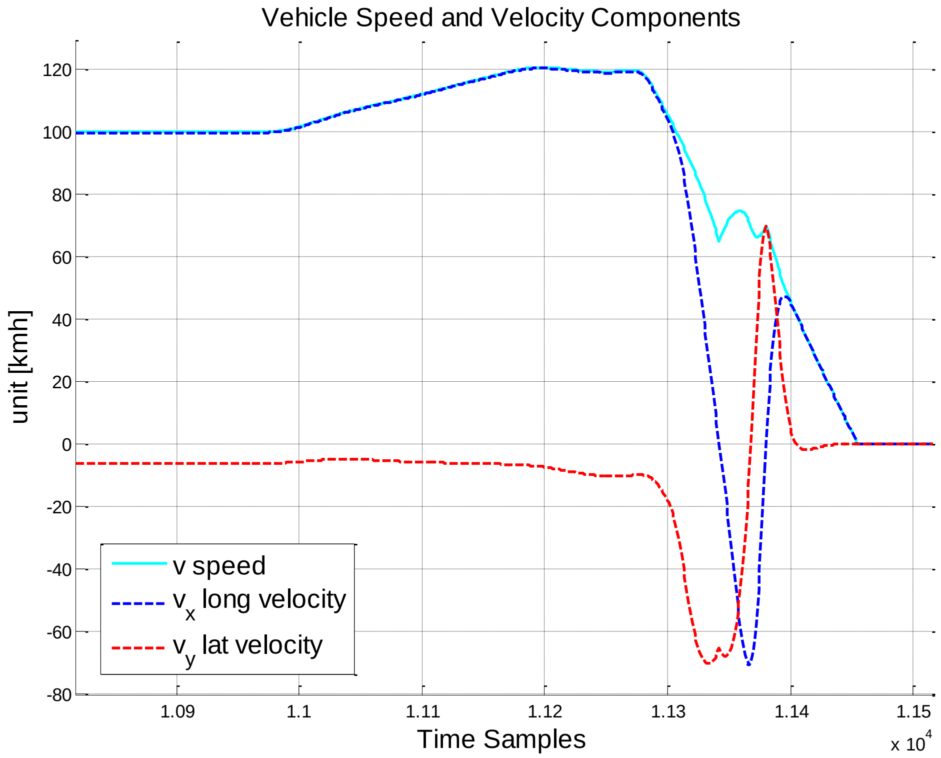

Figure 6.11 Vehicle speed and velocity components under braking from maximum speed in high speed section of modified NEDC, μ 0.4 and 90% rear bias braking strategy

Figure 6.12 is the rear tire/axle friction utilization plot. It can be clearly seen that the tire saturates under braking from maximum speed of the cycle and results in instability as shown in Figure 6.10.

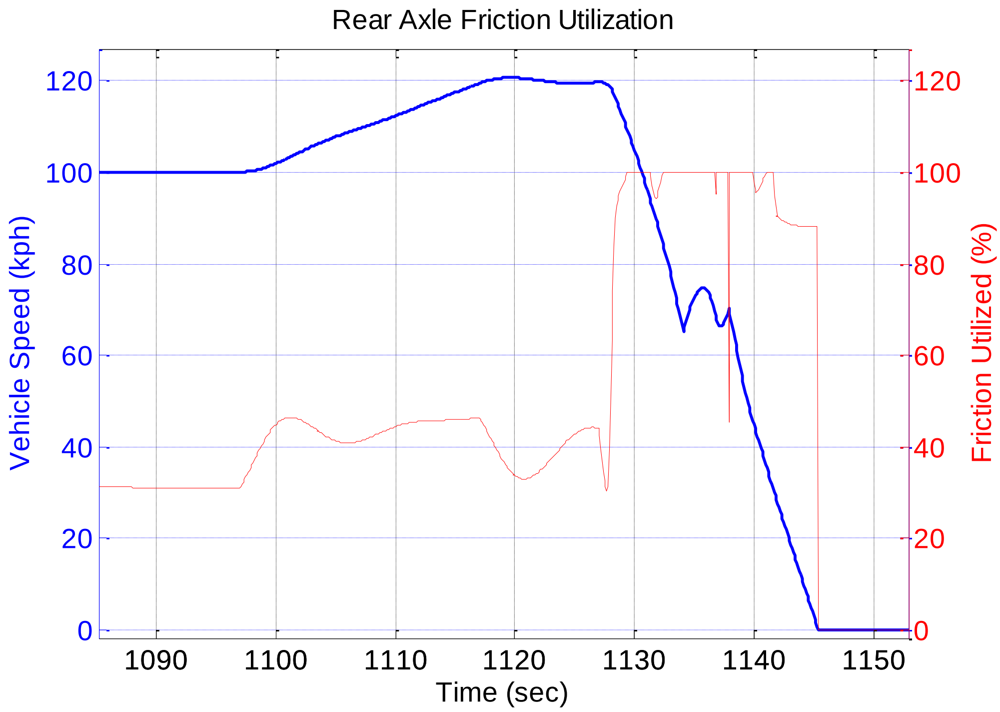

Figure 6.12 Friction utilization under braking from maximum speed in high speed section of modified NEDC, μ 0.4 and 90% rear bias braking strategy

7 Discussion

The size of the electric motor used is 100 kW. This value is relatively high and the extent in which it is representative for current hybrid or electric vehicle is arguable. Lower energy recuperation values would occur with a smaller size motor. However, the size was well suited for the purpose of validating the model and verifying if the evaluation method chosen works.

The integration of the lateral dynamics in the model requires more extensive changes in terms of structure and number of variables.

The modified NEDC cycle is better than the original for differentiating between different brake regeneration strategies both in terms of fuel consumption and vehicle stability. From an OEM's perspective, optimising the system purely for standardized tests is a tempting but risky strategy. Hybrid and electric vehicles are expected to be robust and stable in a wide variety of utilisation conditions. Positive, or even more so, negative feedback from real life utilisation scenarios could prove to be significant for the success of a model.

8 Conclusions

Longitudinal dynamics model

The model extension succeeds in providing a platform for efficiently evaluating different RBS strategies with respect to energy recuperation and vehicle longitudinal & lateral behavior.

A driving cycle better suited for evaluating regenerative braking was needed, the adopted solution being a modified, higher decelerations, NEDC

More than double the energy recuperation is achieved in the tested configuration by biasing the brake distribution 90% to the rear, driven axle. The resulting energy consumption reduction is more than 6 percent,

Energy recuperation and vehicle stability indicators significantly worsen when the available friction is lowered, especially for $\mu < 0.6$.

Longitudinal + lateral dynamics model

Two additional evaluation criteria of vehicle dynamics successfully created.
The same vehicle stability trends from the pure longitudinal dynamics model are encountered when adding lateral dynamics.

For the radius chosen of 800m, the vehicle become unstable in the final section of modified NEDC cycle (high speed section) in low friction conditions ($\mu = 0.2 - 0.5$). For future work, adding corrective steering through feedback based on the yaw rate error could resolve the instability and also open up the opportunity for a path tracking driver model.

The curvature has a significant impact on energy consumption and brake energy recuperation. For $\mu = 1$, the energy recuperation is reduced by 7.5% for both the strategies compared to the results from longitudinal model. And for $\mu = 0.2$, energy recuperation is reduced by 28% for optimal braking strategy and 46% for 90% rear biased braking strategy.

9 Future work

Apart from test cases looked at in this thesis, the models could be used to analyse other braking strategies as well. One of the most interesting ones is a steering sensitive algorithm, were the amount bias towards the axle with regenerative braking is varied depending on the steering angle of the vehicle. Such a strategy was also proposed in (Boerboom 2012).

Implementing a single track vehicle model was the first step for including lateral dynamics aspects such as yaw instability. Interesting additional aspects such as the influence of lateral load transfer or wheel differential braking, individual wheel motors would require a more complex two track vehicle model.

If a more realistic curvature profile is desired (instead of a fixed steering wheel angle), steering feedback should be incorporated in the driver model and used for a feedback control of the vehicle path.

Tire forces are calculated by pure longitudinal $F_X(\kappa)$ and lateral $F_y(\alpha)$ magic formula. For future work, calculating forces from combined slip effect ($F_X(\kappa, \alpha)$ and $F_Y(\alpha, \kappa)$) will improve the assessment of stability.

10 References

Boerboom, Max. 2012. 'Electric Vehicle Blended Braking maximizing energy recovery while maintaining vehicle stability and maneuverability', master's thesis, Chalmers University of Technology.

Bosch. 'Regenerative braking systems', Accessed May 13, 2016. http://www.bosch.de/media/de/germany/rich_media/electromobility_1/electromobility_download/pdf/electromobility_brochure_consumption_en.pdf.

DeNovellis, Leonardo, Aldo Sorniotti, Patrick Gruber, Leo Shead, Valentin Ivanov, and Kristian Hoepping. "Torque Vectoring for Electric Vehicles with Individually Controlled Motors: State of the art and Future Developments." In *EVS26 International Battery, Hybrid and Fuel Cell Electric Vehicle Symposium*. Los Angeles.

Heißing, Bernd, and Metin Ersoy. 2011. *Chassis Handbook* (Springer Fachmedien Wiesbaden GmbH: Berlin).

Jacobson, Bengt. 2014. *Vehicle Dynamics Compendium* (Department of Applied Mechanics, Chalmers University of Technology).

Klomp, M., and R. Thomson. 2011. 'Influence of front/rear drive force distribution on the lateral grip and understeer of all-wheel drive vehicles', *International journal of vehicle design*, 56.

Marotta, Alessandro, Jelica Pavlovic, Biagio Ciuffo, Simone Serra, and Georgios Fontaras. 2015. 'Gaseous Emissions from Light-Duty Vehicles: Moving from NEDC to the New WLTP Test Procedure', *Environmental Science and Technology*.

Mutoh, Nobuyoshi. 2012. 'Driving and Braking Torque Distribution Methods for Front- and Rear-Wheel-Independent Drive-Type Electric Vehicles on Roads With Low Friction Coefficient', *IEEE TRANSACTIONS ON INDUSTRIAL ELECTRONICS*, 59.

Pacejka, Hans. 2012. *Tire and Vehicle Dynamics* (Butterworth-Heinemann).

Parker, G., J. Griffin, and A. Popov. 2016. "The effect on power consumption & handling of efficiency-drivern active torque distribution in a four wheeled vehicle." In *24th Symposium of the International Association for Vehicle System Dynamics*. Graz, Austria: Taylor & Francis Group.

Schmid, Markus. 2011. 'Tire Modeling for Multibody Dynamics Applications', University of Wisconsin - Madison.

Sjunnesson, Ingrid, Rudolf Brziak, and Meng Yao. 2015. "Documentation of Energy Model v2.5." In.: LeanNova.

UnitedNations. 2011. "Uniform provisions concerning the approval of passenger cars with regard to braking." In *Addendum 12-H: Regulation No. 13-H*.

11 Appendix (ÅF internal documents)

11.1 A1 Model utilisation instructions (1)

11.2 A2 Model revision history (1)

11.3 A3 Model utilisation instructions (2)

11.4 A4 Model revision history (2)